AGU ADVANCING EARTH AND SPACE SCIENCE

Water Resources Research

RESEARCH ARTICLE
10.1029/2020WR027192

Key Points:
- Detailed concentration profiles reveal grain-size specific density stratification
- Sediment diffusivity effects are overwhelmed by density stratification at high concentrations
- Fine washload sediment (<25 μm) is vertically stratified in the Yellow River

Supporting Information:
- Supporting Information S1

Correspondence to:
A. J. Moodie,
amoodie@rice.edu

Citation:
Moodie, A. J., Nittrouer, J. A., Ma, H., Carlson, B. N., Wang, Y., Lamb, M. P., & Parker, G. (2020). Suspended sediment-induced stratification inferred from concentration and velocity profile measurements in the lower Yellow River, China. *Water Resources Research*, *56*, e2020WR027192. https://doi.org/10.1029/2020WR027192

Received 21 JAN 2020
Accepted 6 OCT 2020
Accepted article online 14 OCT 2020

Suspended Sediment-Induced Stratification Inferred From Concentration and Velocity Profile Measurements in the Lower Yellow River, China

Andrew J. Moodie[1], Jeffrey A. Nittrouer[1], Hongbo Ma[1], Brandee N. Carlson[1], Yuanjian Wang[2], Michael P. Lamb[3], and Gary Parker[4,5]

[1]Department of Earth, Environmental and Planetary Sciences, Rice University, Houston, TX, USA, [2]Yellow River Institute of Hydraulic Research, Zhengzhou, China, [3]Division of Geological and Planetary Sciences, California Institute of Technology, Pasadena, CA, USA, [4]Department of Civil and Environmental Engineering, University of Illinois at Urbana-Champaign, Champaign, IL, USA, [5]Department of Geology, University of Illinois at Urbana-Champaign, Champaign, IL, USA

Abstract Despite a multitude of models predicting sediment transport dynamics in open-channel flow, self-organized vertical density stratification that dampens flow turbulence due to the interaction between fluid and sediment has not been robustly validated with field observations from natural rivers. Turbulence-suppressing density stratification can develop in channels with low channel-bed slope and high sediment concentration. As the Yellow River, China, maintains one of the highest sediment loads in the world for a low sloping system, this location is ideal for documenting particle and fluid interactions that give rise to density stratification. Herein, we present analyses from a study conducted over a range of discharge conditions (e.g., low flow, rising limb, and flood peak) from a lower reach of the Yellow River, whereby water samples were collected at targeted depths to measure sediment concentration and, simultaneously, velocity measurements were collected throughout the flow depth. Importantly, sediment concentration varied by an order of magnitude between base and flood flows. By comparing measured concentration and velocity profiles to predictive models, we show that the magnitude of density stratification increases with sediment concentration. Furthermore, a steady-state calculation of sediment suspension is used to determine that sediment diffusivity increases with grain size. Finally, we calculate concentration and velocity profiles, showing that steady-state sediment suspensions are reliably predicted over a range of stratification conditions larger than had been previously documented in natural river flows. We determine that the magnitude of density stratification can be predicted by a function considering an entrainment parameter, sediment concentration, and bed slope.

1. Introduction

The development and effects of density stratification in natural rivers are not sufficiently documented to validate sediment suspension models over a range of river discharges and grain sizes (e.g., de Leeuw et al., 2020; García, 2008). Suspended sediment in a flow creates a stable stratification, because higher sediment-induced effective density is located near the channel bed (Einstein & Chien, 1955; Turner, 1979; Vanoni, 1941; 1946; Villaret & Trowbridge, 1991). However, turbulent mixing disrupts density stratification, rendering it weak and often ephemeral in rivers (e.g., Minier et al., 2014; van Rijn, 1984). Measurements of stratification dynamics are limited, and so physical models are under constrained (Bolla Pittaluga, 2011; Minier et al., 2014; Wright & Parker, 2004a; Yeh & Parker, 2013). This research aims to assess predictions of flow velocity and sediment concentration dynamics, thereby testing and calibrating models for studies that seek to constrain sediment fluxes in lowland rivers and coastal deltas (Ma et al., 2020; Meselhe et al., 2012; Xu et al., 2019).

Sediment discharge in large, low-gradient rivers is dominated by suspended transport (Ma et al., 2017; Milliman & Meade, 1983; Nittrouer et al., 2008) and thus may be modulated by density stratification.

Suspended load is estimated by integrating the product of width-averaged velocity and concentration profiles over the flow depth:

$$q_s = \int^{H} \bar{u}(z)\bar{c}(z)\,dz, \tag{1}$$

where z is a quasi-vertical coordinate (i.e., assuming a low channel slope), H is the flow depth, $\bar{u}$ is the streamwise velocity (averaged over the turbulent eddy integral timescale, which is related to the spatial extent [water depth] and velocity of eddies), and $\bar{c}$ is the volumetric sediment concentration (averaged over the turbulent eddy integral timescale) (García, 2008). Thus, accurate prediction of sediment transport in low-gradient rivers and delivery to coastal deltas requires determining velocity and suspended sediment concentration depth-profiles from adequately calibrated models. However, data from natural rivers covering exceptionally high sediment concentration and fine grain size are lacking in existing literature.

Traditionally, models of velocity and concentration assume a dilute suspension (Rouse, 1937), whereby particles do not modulate flow. In these models, turbulent stresses are assumed to be related to the mean flow (Boussinesq approximation Landau & Lifshits, 1959), and the Prandtl mixing-length analogy can be utilized to close turbulent fluxes. The mixing length concept describes an eddy viscosity mixture profile (K_m) that varies parabolically with distance above the bed (Doshi & Gill, 1970; Landau & Lifshits, 1959; Rouse, 1937):

$$K_m = \kappa u_* z(1 - (z/H)), \tag{2}$$

where $u_* = \sqrt{\tau_b/\rho}$ is the fluid shear velocity (a representation of basal shear stress τ_b in units of L T^{-1}, where ρ is fluid density) and $\kappa = 0.41$ is the von Kármán constant (Einstein & Chien, 1955; Nezu & Rodi, 1986). Numerous researchers have tested dilute suspension velocity and concentration profile models with data collected from laboratory experiments (Lyn, 1986; van Ingen, 1981; Vanoni, 1941), the field (Anderson, 1942; Barton & Lin, 1955; Colby, 1964; Colby & Hembree, 1955), and through numerical simulations (Amoudry, 2005; Chan-Braun et al., 2010; Hsu et al., 2004; Schmeeckle, 2014). These studies have determined that suspended sediment increases the effective density of the fluid and higher sediment concentration near the bed produces a vertical density gradient that induces a negative buoyancy that modulates eddy viscosity by increasing the dissipation of turbulent eddies. Hence, density stratification limits redistribution of momentum and sediment and invalidates the Prandtl mixing length assumption and parabolic eddy viscosity profile (Equation 2 Lyn, 1986; Parker & Coleman, 1986; van Rijn, 1984; Villaret & Trowbridge, 1991; Wright & Parker, 2004a).

Many studies have developed parameterizations of density stratification (Gelfenbaum & Smith, 1986; McLean, 1991, 1992; Munk & Anderson, 1948; Smith & McLean, 1977; Villaret & Trowbridge, 1991), because representing multiple physical processes via a small number of parameters is analytically and computationally convenient (Wright & Parker, 2004b). In particular, several parameterizations apply a depth-averaged correction to the eddy viscosity profile (Einstein & Chien, 1955; Mofjeld, 1988; Wright & Parker, 2004b):

$$K_m = \alpha\kappa u_* z(1 - (z/H)), \tag{3}$$

where α is a depth-averaged adjustment to the eddy viscosity profile which accounts for density stratification effects. Thus, a clear-water eddy viscosity profile (K_{m0}) is defined by the eddy viscosity adjustment coefficient $\alpha = 1$, and modulating $\alpha < 1$ parameterizes density stratification impact on the redistribution of energy by turbulent eddies.

The density-stratified eddy viscosity profile (Equation 3) can be used to derive velocity and concentration profiles that use the α coefficient to parameterize stratification. The log-law velocity profile for a steady, uniform, and hydraulically rough flow is obtained by integrating the eddy viscosity profile over z and applying an empirical closure for an integration constant $z_0 = k_s/30$:

$$\frac{\bar{u}}{u_*} = \frac{1}{\alpha\kappa} \ln\left(30\frac{z}{k_s}\right), \tag{4}$$

where $k_s = 3D_{90}$ is the roughness height and D_{90} is the 90th percentile of the cumulative grain-size distribution of bed sediment (Mofjeld, 1988; Nikuradse, 1926; van Rijn, 1984).

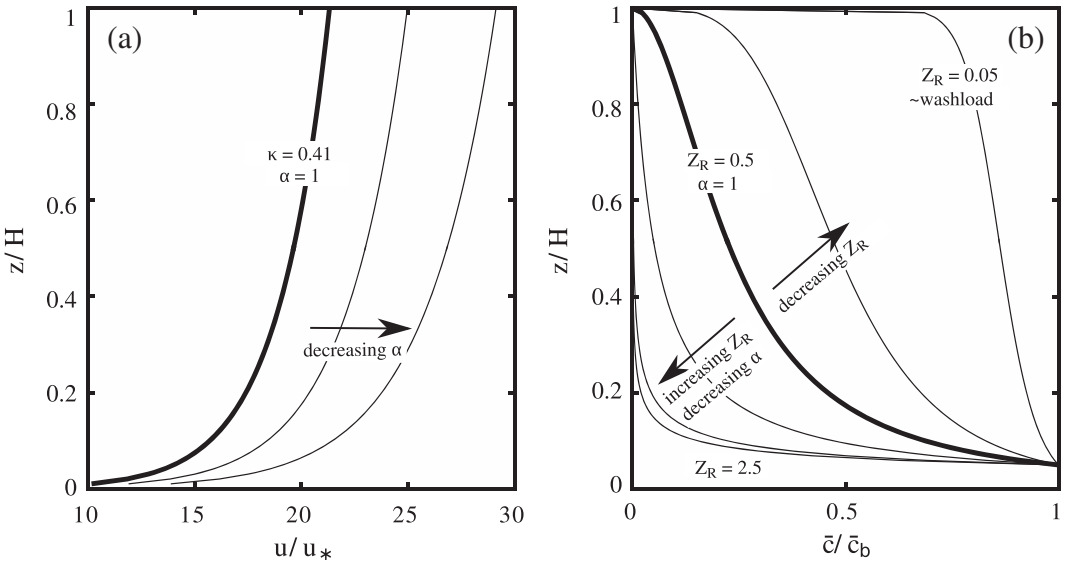

Figure 1. (a) Dimensionless (normalized) log-law velocity profile calculated by Equation 4 for a shear velocity $u_* = 0.1$ m/s, flow depth $H = 3$ m, and roughness height $k_s = 4.8 \times 10^{-4}$ m. A decrease in α causes an increase in the velocity gradient. (b) Dimensionless (normalized) Rouse profiles calculated by Equation 5. A decrease in α increases the Rouse number.

The vertical profile of sediment concentration for grain size i follows from sediment mass conservation over vertical sediment movement: upward advection turbulent eddies and grain settling due to gravity (Mofjeld, 1988). For steady-state vertical sediment movement (Rouse, 1937),

$$\frac{\bar{c}_i}{\bar{c}_{bi}} = \left[\frac{(H-z)/z}{(H-b)/b}\right]^{Z_{Ri}}, \tag{5}$$

$$Z_{Ri} = \frac{w_{si}}{\alpha\kappa u_*}, \tag{6}$$

where $\bar{c}_{bi}$ is the near-bed concentration for grain size i (at $z = b$, where b is a near bed elevation, herein set to 5% of the flow depth above the bed, after Wright & Parker, 2004a) averaged over the turbulent eddy integral timescale, and Z_{Ri} is the Rouse number for grain size i. The Rouse number characterizes the steady-state balance between particle settling velocity (w_{si}) and the upward advection of sediment by turbulent eddies, which scales with shear velocity (u_*) (Figure 1b; Rouse, 1937; Vanoni, 1946). As $Z_R \to \infty$, sediment is concentrated near the bed, and as $Z_R \to 0$, sediment concentration is vertically uniform (Figure 1b).

In addition to density stratification effects, the vertical concentration profile may be affected by sediment diffusivity, which approximates the efficiency of momentum transfer from turbulent fluid to suspended sediment (Rouse, 1937, 1939). The Rouse sediment concentration profile model (Equation 5) assumes that sediment diffusivity is equal to the kinematic eddy viscosity, whereby the sediment diffusivity coefficient $\beta = K_s/K_m = 1$ (Rouse, 1937, 1939). This formulation implies that sediment diffusivity is not independent from density stratification, because density stratification also depends on the eddy viscosity (K_m), which is itself modulated by stratification. As a result, the effects of density stratification and sediment diffusivity variability are implicitly assumed to interact linearly for analyses using a depth-averaged concentration profile adjustment; in essence, the total profile adjustment = $\alpha\beta$.

The effect of sediment diffusivity may be separated from density stratification by pairwise comparison of concomitant velocity and concentration profiles. The value of sediment diffusivity β is frequently debated (Cellino & Graf, 1999; Coleman, 1970; Graf & Cellino, 2002; Jobson, 1970; Lees, 1981; Murray, 1970; Rose & Thorne, 2001; Schmeeckle, 2014; van Rijn, 1984; Whitehouse, 1995). Some suggest that higher sediment inertia (due to greater density) prevents an immediate response to turbulent velocity fluctuations ($\beta < 1$). Alternatively, higher sediment momentum could also thrust particles from eddies and thus have a diffusive effect ($\beta > 1$). In actuality, the value of β likely varies with depth and is dependent on both grain size and

sediment concentration (Amoudry, 2005; Cellino & Graf, 1999; Ghoshal & Pal, 2014; Graf & Cellino, 2002; Greimann & Holly, 2001; Greimann et al., 1999; Lees, 1981).

Finally, the strength of sediment-induced stratification is limited by the near-bed sediment concentration, which is determined, in part, by the rate of sediment entrainment from the bed into the flow (E_r). However, it is unclear how turbulent dampening modulates sediment entrainment itself. Intuitively, it may be expected that the sediment entrainment rate is reduced by dampening of turbulence intensity and magnitude of entraining turbulent eddies; yet, a near-bed sediment-laden fluid layer could minimize drag from the channel bed and thus sustain a shear velocity consistent with an unstratified flow (Toorman, 2002; Vanoni, 1941; Wang & Larsen, 1994). In any case, turbulent energy is consumed by the near-bed density gradient over a shortened length (height) scale when concentration is increased (e.g., García & Parker, 1991, 1993).

Entrainment can be quantified by measuring the steady-state near-bed concentration. Net vertical sediment flux near the bed depends on the balance of upward flux of sediment from the bed (the entrainment rate, E_r) that depends on transport stage, and a downward flux (the deposition rate, D_r) that depends on sediment concentration and settling velocity:

$$\bar{F}_{z=b} = E_r - D_r = w_s(E_s - \bar{c}_b), \tag{7}$$

where $E_s \equiv E_r/w_s$ is a dimensionless entrainment rate (i.e., volume per-unit-bed-area per unit time García, 2008). So, at steady state, the net sediment flux ($\bar{F}_{z=b} = 0$) is zero, and the dimensionless entrainment rate is equivalent to the near-bed concentration, $E_s = \bar{c}_b$. The entrainment reference height is assumed to be the same height as the near-bed concentration boundary condition for vertical concentration profile modeling (5% of the flow depth above the bed). As transport stage of the flow changes, entrainment and the near-bed concentration are expected to change, but the effect of density stratification on entrainment has not been explored experimentally or with data from natural open-channel flows.

Despite a clear theoretical foundation, development of density stratification as a function of water discharge and sediment concentration in natural open-channel flows lacks robust validation due to limited data. Herein, we present measurements of flow velocity and sediment concentration profiles from the Yellow River, China, collected at river discharges varying over several orders of magnitude. We measured the grain-size distribution of each sample to determine the grain-size specific impact of stratification and used these measurements to validate velocity and sediment concentration profile models. In particular, we evaluate various models for concentration profiles in open-channel flow under stratified conditions, the behavior of sediment diffusivity with respect to fluid over flow depth and changes in sediment concentration, and modulation of sediment entrainment rates due to stratification. To our knowledge, this is the most detailed and comprehensive study of density stratification in a natural river system, to date.

Measuring relevant flow and sedimentologic parameters is necessary to validate density stratification models and effectively isolate density stratification effects (e.g., isolate α in Equation 5). Unfortunately, it is difficult to simultaneously measure each relevant variable in a fast-moving and highly concentrated natural river flow, and so we constrain the flow shear velocity (section 3.3) and treat this as known in subsequent analyses. Moreover, we avoid directly calculating concentration and velocity profile gradients, because these data are limited in the vertical and single measurements carry significant uncertainty. Instead, we evaluate metrics derived by depth integrating (i.e., regression) and depth averaging, which reveals clearer systematic trends in stratification.

2. Background

2.1. Identifying Relevant Physical Terms for Density Stratification Parameterization

The strength of density stratification is quantified in the flux Richardson number (Bolla Pittaluga, 2011; Gelfenbaum & Smith, 1986; McLean, 1991, 1992; Smith & McLean, 1977; Wright & Parker, 2004b), which ratios the energy lost working against a density gradient to the turbulent energy generated by fluid shear:

$$\mathrm{Ri} = \frac{Rg\sum_{i=1} w_{si}\bar{c}_i}{u_*^2(1-(z/H))(d\bar{u}/dz)}, \tag{8}$$

where $R = (\rho_s - \rho)/\rho$ is the submerged specific gravity of sediment, ρ_s is the sediment density, and g is the gravitational acceleration constant (Lamb & Parsons, 2005; Turner, 1979; Wright & Parker, 2004b). A nondimensionalized, depth-averaged, and cumulative grain size (i.e., bulk) version of Equation 8, which assumes

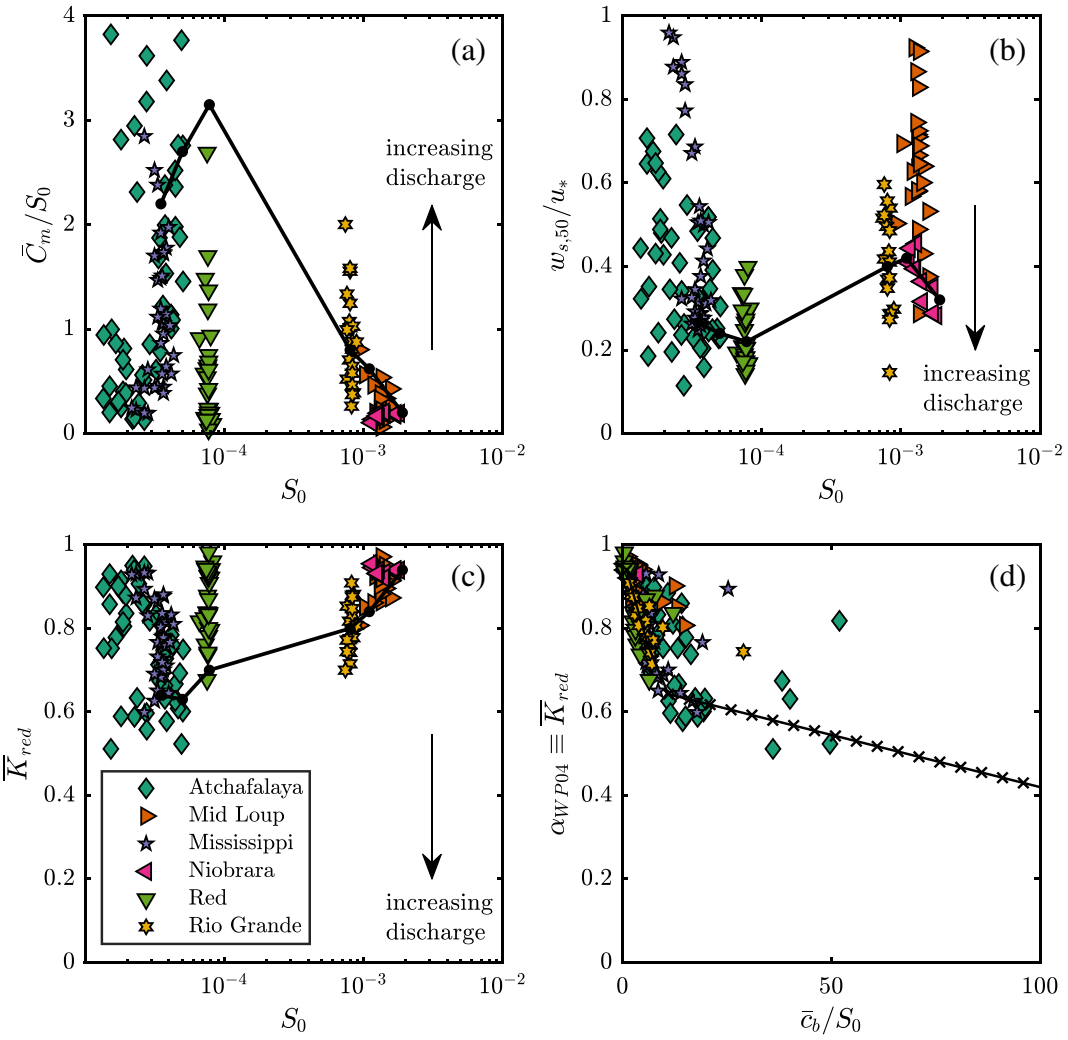

Figure 2. Selected figures after Wright and Parker (2004a, 2004b), displaying trends from six sand-bed rivers, and estimated values at 5% exceedance discharge. (a) Ratio of total discharge-weighted suspended sediment concentration to slope versus slope. (b) Dimensionless settling velocity versus slope. (c) Depth-averaged reduction in eddy viscosity versus slope. (d) Predictive relationship for depth-averaged reduction in eddy viscosity (Equation 10).

stationary and uniform flow, is given by the sand-river Richardson number (Wright & Parker, 2004a):

$$\mathrm{Ri}_{\mathrm{sr}} = R\frac{w_{s,50}}{u_*}\frac{\bar{C}}{S_0}, \tag{9}$$

where $\bar{C}$ is the discharge-weighted sediment concentration and S_0 is the water-surface slope.

Dimensional analysis of an alternative velocity and concentration profile model formulation retaining buoyancy effects (Mellor & Yamada, 1982; Villaret & Trowbridge, 1991) demonstrates that density stratification is governed by the terms comprising the sand-river Richardson number (Equation 9 Wright & Parker, 2004a): the sediment dimensionless settling velocity (w_s/u_*), sediment concentration ($\bar{C}$), and water-surface slope (S_0). The sand-river Richardson parameters from several natural rivers show that the dimensionless settling velocity ($w_{s,50}/u_*$) varies independently of discharge and slope (Figure 2b). In contrast, the ratio of discharge-weighted sediment concentration to slope ($\bar{C}/S_0$; Figure 2a) increases significantly from low to high discharge in low-sloping rivers, but only mildly in steeper rivers. Further, a reduction in the depth-averaged eddy viscosity correlated with a decrease in $\bar{C}/S_0$ ratio (Figure 2c) indicates that a low channel bed slope enhances density stratification effects (Wright & Parker, 2004a). However, for a given river, sediment concentration may vary by up to two orders of magnitude, whereas slope varies minimally over a wide range of discharges (Figure 2a). Thus, while the maximum strength of density stratification observed is

modulated by the channel-bed slope, the actual magnitude of density stratification is principally dependent on sediment concentration.

2.2. Parameterized Concentration Profile Adjustment and the Buoyancy-stratified Model

Here, the eddy viscosity profile adjustment from Wright and Parker (2004a) is used: Let $\bar{K}_{red} = \bar{K}_m/\bar{K}_{m0}$, the ratio of the depth-averaged sediment-laden fluid eddy viscosity ($\bar{K}_m$) to the depth-averaged clear-water eddy viscosity ($\bar{K}_{m0}$). Wright and Parker (2004b) cast the depth-averaged eddy viscosity reduction as the density-stratification adjustment coefficient α_{WP04} (i.e., $\alpha_{\mathrm{WP04}} \equiv \bar{K}_{red}$; Figure 2d):

$$\alpha_{\mathrm{WP04}} = \begin{cases} 1 - 0.06(\bar{c}_b/S_0)^{0.77} & \text{for } (\bar{c}_b/S_0) \le 10 \\ 0.67 - 0.0025(\bar{c}_b/S_0) & \text{for } (\bar{c}_b/S_0) > 10 \end{cases}. \tag{10}$$

Decreasing α increases the vertical velocity stratification and lowers the suspended sediment concentration.

The observations used to develop α_{WP04} (Equation 10) arise from applying a buoyancy-stratified model to solve for a sediment concentration profile that reproduced depth-averaged concentration measurements from literature (Wright & Parker, 2004a, 2004b, and references therein). The buoyancy-stratified model employs a turbulence closure scheme derived from the full Reynolds transport equations, which omits advection and diffusion components in all terms except the turbulent kinetic energy equation and therefore assumes that Reynolds-averaged turbulent characteristics are in local equilibrium (the "Level 2-1/2" model Galperin et al., 1988; Mellor & Yamada, 1982; Yeh & Parker, 2013). We use the buoyancy-stratified model as detailed by Yeh and Parker (2013).

The buoyancy-stratified model has not been rigorously tested against concentration or velocity profiles from natural river systems. Nevertheless, parameterized adjustment to concentration profiles via the α coefficient are regularly leveraged in geomorphology studies (e.g., Lamb et al., 2012; Nittrouer et al., 2011, 2012; Viparelli et al., 2015). Thus, the density stratification models and analyses from Wright and Parker (2004a, 2004b) provide an important point of comparison throughout our study, because the approaches and results have been widely applied since publication (e.g., Fildani et al., 2006; Lamb et al., 2008; McElroy & Mohrig, 2009; Wright & Parker, 2005).

2.3. Sediment Entrainment

Many entrainment relations exist in the literature, with a wide range of necessary parameters (reviewed in de Leeuw et al., 2020; García, 2008). The relations are typically of the form $E_s = f(\tau_b, D, \dots)$, where parameters other than τ_b and D include critical stress of mobility (τ_{cr}), slope (S), and/or Richardson number (Ri) (García, 2008; van Rijn, 1984). Here, we focus on a relation that incorporates the effects of density stratification through a dependence on the channel bed slope (Wright & Parker, 2004b):

$$E_{si} = \frac{B\left(\lambda X_i\right)^5}{1 + \frac{B}{0.3}(\lambda X_i)^5}, \tag{11}$$

$$X_i = \left(\frac{u_*}{w_{si}}\mathrm{Re}_{\mathrm{pi}}^{0.6}\right) S_0^{0.08}\left(\frac{D_i}{D_{50}}\right)^{0.2}, \tag{12}$$

where X_i is the entrainment parameter of grain class i, $\lambda = 1 - 0.28\sigma_\phi$, where σ_ϕ is the standard deviation of the channel-bed sediment in the sedimentological ϕ scale; $B = 7.8 \times 10^{-7}$ is an empirical parameter; $\mathrm{Re}_{pi} = \left(\sqrt{RgD_i}D_i\right)/\nu$ is the particle Reynolds number of grain class i, where ν is the kinematic viscosity of the fluid; D_i is the characteristic diameter of grain-class i; and D_{50} is the median grain diameter of the bed sediment (García & Parker, 1991, 1993); note that the original reference uses the skin friction component of shear velocity (Wright & Parker, 2004b). Recall that the near-bed concentration and dimensionless entrainment rate are equivalent at steady state ($E_s = \bar{c}_b$); therefore, the reference concentration and height are determined at 5% of the flow depth above the bed (Wright & Parker, 2004a). A potential problem with this approach is that density stratification effects are then fixed for a given slope (in contrast to data observations in Figure 2b; Wright & Parker, 2004a). This entrainment relation (Equation 12) thus provides some consideration of density stratification effects; however, it is not clear whether this will capture the full range of density stratification in a river.

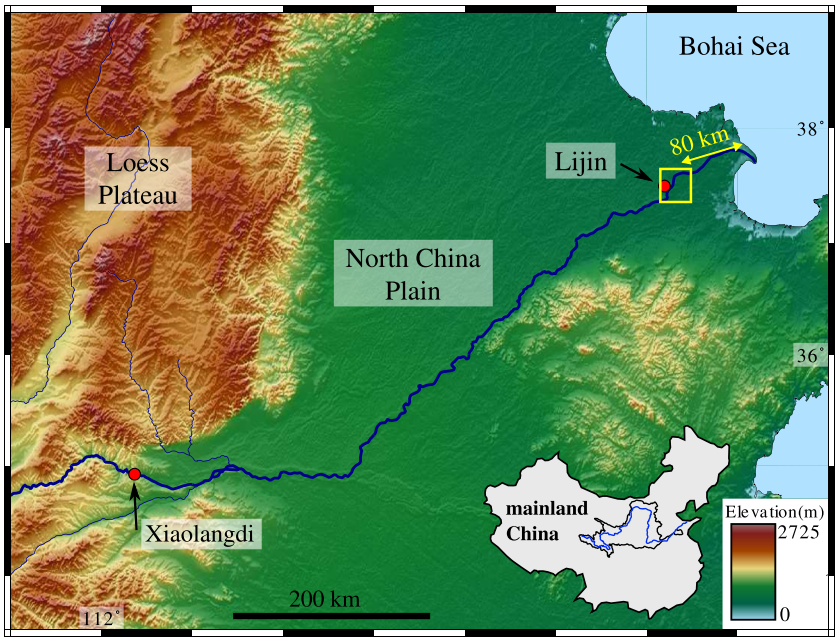

Figure 3. Map of the lower Yellow River; inset shows drainage basin and course of Yellow River across mainland of China. The study area is 80–100 km upstream of the river mouth, and the yellow box contains the map areas shown in Figure 4.

3. Yellow River Fluvial System

Density stratification is expected to develop in low-slope and high sediment concentration flows (Wright & Parker, 2004a). The Yellow River is thus an ideal natural laboratory to explore the development and effects of density stratification on hydrodynamics and sediment transport. The Yellow River flows across northern China, generally from west to east, draining an area of 752,000 km^2 over a river length of 5,460 km, before entering the Bohai Sea (Figure 3) (Ren & Walker, 1998; Saito et al., 2000; van Gelder et al., 1994). The drainage basin includes the Loess Plateau, an unconsolidated sediment deposit ~100 m thick composed of very fine sand and silt (Ma et al., 2017; Saito et al., 2001; Yu, 2002), which is readily eroded and contributes to the large sediment discharge of the Yellow River (1 Gt/year Yu, 2002). With a bankfull discharge of 3,000–4,000 m^3/s, sediment concentration in the lower Yellow River is remarkably high, approximately 1 to 2 orders of magnitude greater than other large lowland rivers (e.g., Mississippi River and Amazon River) (Wang & Liang, 2000; Yu, 2002). In the lower Yellow River (lowermost ~200 km) bankfull flow depth ranges 2–6 m, and channel width averages 400 m. Channel bed slope in the lower Yellow River takes the approximately constant value 6.4×10^{-5} (Moodie et al., 2019). Yellow River sediment concentration varies by several orders of magnitude as a function of water discharge (Ma et al., 2017; Moodie et al., 2019), which provides the opportunity to study development of density stratification with progressively changing sediment concentration.

3.1. Field Measurements

Three field campaigns in the summers of 2015, 2016, and 2018 were conducted between 80 and 100 km upstream of the river mouth, near the cities of Kenli and Lijin (Figures 3 and 4a; Moodie, 2019). This straight reach of channel is upstream of backwater influence and away from any significant changes in channel-bed slope (Ganti et al., 2014; Moodie et al., 2019); we therefore do not expect any systemic spatial disequilibrium due to river hydraulics or bed composition. Field survey objectives included collecting water column velocity and concentration measurements over a range of water discharge conditions from 21 stations (Figure 4). Measurements at a single time-space window spanned less than 1 hr, and so for the purposes of our calculations, we assume constant hydrographic conditions for a survey (i.e., steady flow).

During the 2015 survey, a single point-integrated water sample (1 L) was collected at three fixed heights above the bed ($z/H = 0.05$, 0.25, and 0.5), and a channel bed grab sediment sample was collected to assess bed material grain size (Figure 5a). In the 2016 and 2018 surveys, a bed sediment sample and three water and suspended sediment samples were collected at five points above the bed ($z/H = 0.05$, 0.15, 0.25, 0.5,

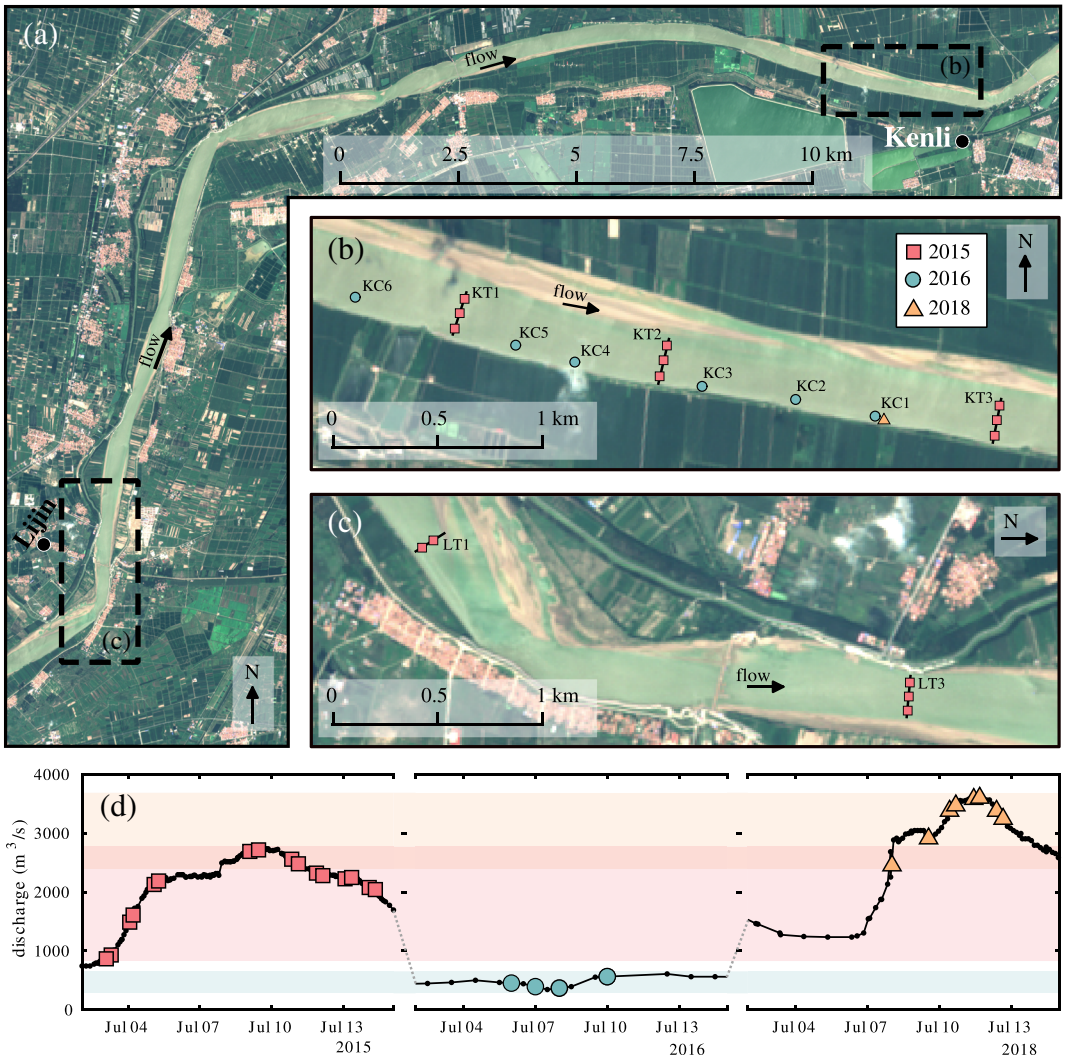

Figure 4. (a) Overview of survey reaches from this study, Lijin (upstream) and Kenli (downstream), located ~24 km from one another. (b) Field survey map of the Kenli survey reach. KT refers to a transect along which three stations are located (2015 survey). KC refers to a station from 2016 or 2018. (c) Field survey map of the Lijin survey reach. LT refers to a transect along which two to three stations are located (2015). Images from Sentinel 2 satellite, 10 February 2016. (d) Composite hydrograph from three survey years; symbols denote timing of station surveys, which cover the full range of the hydrograph.

and 0.9) for a total of 15 water samples at each station (Figures 5b and 5c). Suspended sediment samples were collected using a temporal window of 15–30 s, which is longer than the expected eddy integral time scale, such that the coherent flow structure does not cause measured values to deviate significantly from averaged measurements. Three samples collected at each height provided a means to accurately constrain the mean sediment concentration and grain-size distribution in the flow (Gitto et al., 2017). For all survey years, samples collected at 5% of the flow depth above the bed ($z/H = 0.05$) are reference concentrations used in subsequent analyses.

Water samples were processed to determine sediment concentration by measuring total sample water volume, weighing the dried samples, and assuming a sediment density of 2,650 kg/m^3. The grain-size distribution of each sample (suspended sediment and channel bed samples) was determined by laser diffraction in a Malvern Mastersizer 2000 instrument. After measurement, the fraction of the suspended sediment samples finer than 15 μm was analytically excluded from subsequent analyses (Figures 5a–5c; Ma et al., 2017), and the grain-size distributions were renormalized and cast into a logarithmically spaced six-class distribution. The finest fraction of the grain-size distribution (<15 μm) was removed because sediment in this size

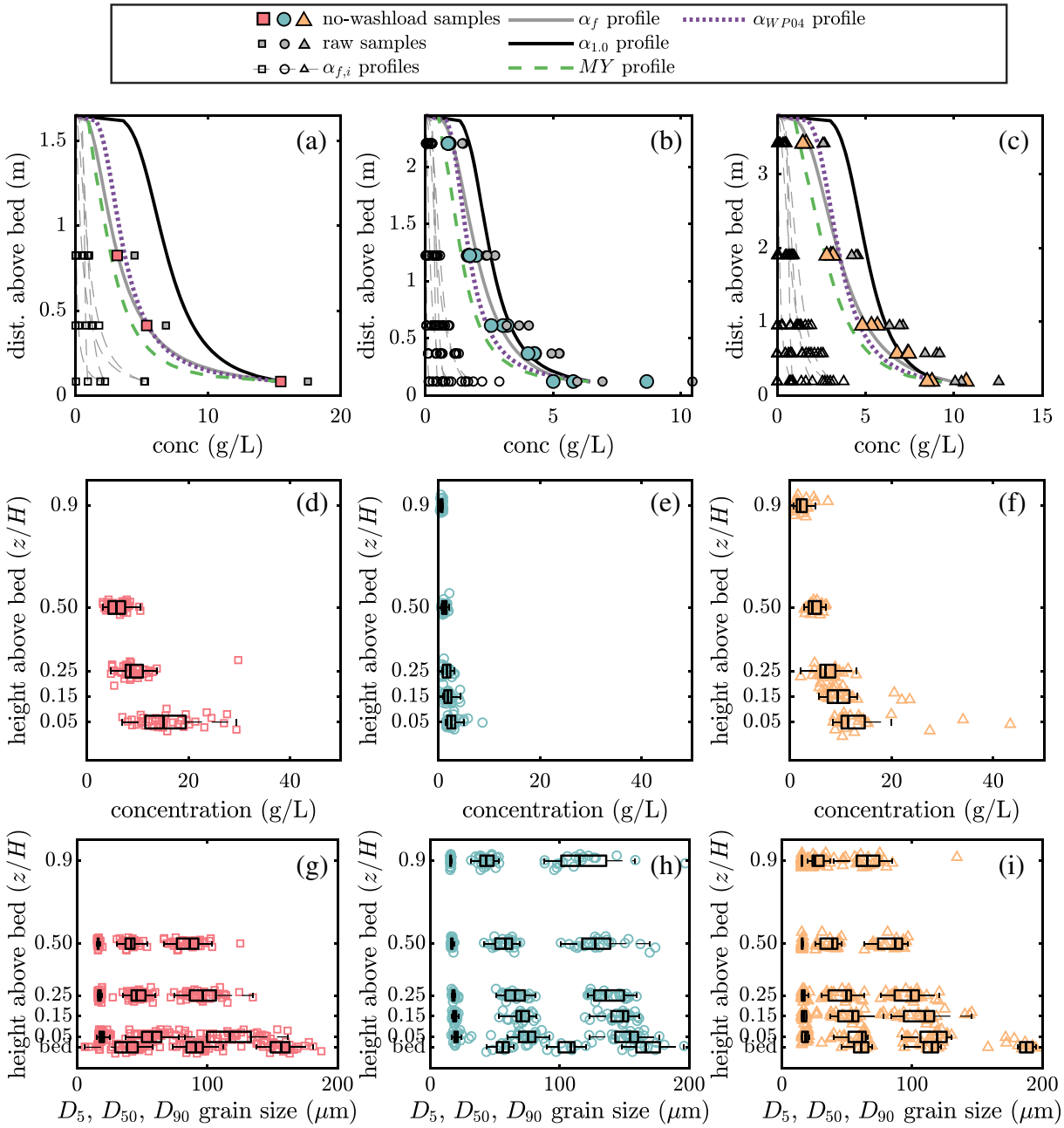

Figure 5. (a–c) Representative 2015, 2016, and 2018 stations with sediment concentration measurements and modeled profiles. Small gray symbols are measured water-sediment samples, filled symbols are samples after removing the sediment fraction finer than 15 μm, thick gray line is the summed profile of grain-size specific best fit concentration profile models (thin gray lines), black solid line is prediction based on α-stratified concentration profile model without density stratification effects (Equations 5 and 6; $\alpha = 1$), and black dashed line is buoyancy-stratified model evaluated for the station. (d–f) Boxplots of sediment concentration as a function of normalized collection height, for each survey year. (g–i) Boxplots of D_5, D_{50}, and D_{90} for all suspended sediment and channel-bed samples, for each survey year.

range likely do not reflect local hydraulic and sedimentologic conditions, therefore leading to erroneous data values (Partheniades, 1977; Woo et al., 1986); we present a discussion of "washload" size sediment later in the text (section 5.3). Stations where the concentration profile did not monotonically increase with depth were identified as outliers ($n = 7$ out of 54).

Sample processing resulted in more than 1,700 grain-size specific sediment concentration measurements that span the range of flow depth and discharge of the lower Yellow River. In order to evaluate the data on a per-station basis, the cumulative concentration profile (i.e., total of all grain-size classes) is characterized

given the median bed-material grain size. For all calculations herein, grain settling velocity is computed via Dietrich (1982).

3.2. Survey Measurements

The samples in this study are all collected from the same reach; water surface slope, $S_0 = 6.4 \times 10^{-5} \pm 3.6 \times 10^{-6}$, is measured from a shipboard navigation system (Moodie et al., 2019). Measured sediment concentration from all surveys are shown in Figures 5d–5f. Floods during the 2015 and 2018 field surveys (>2,000 m^3/s) generated near-bed sediment concentration in excess of 30 g/L. In contrast, without a flood, the near-bed concentration during the 2016 survey is, on average, 80% lower than 2015 and 2018. Overall, the measured concentration decreases with increasing distance above the bed (Figures 5d–5f). Multiple samples collected from the same depth show little variability in concentration or grain-size distribution (Figure 5), which provides evidence that the concentration profiles reflect values averaged over the turbulent eddy integral timescale (15–30 s).

The median grain size of the bed sediment is 90–120 μm across all survey years (Figures 5g–5i). Bed material samples from 2015 are finer than 2016 and 2018. This may be the result of a different collection device that inadvertently introduced very fine suspended sediment into bed samples in 2015. Overall, the grain-size distributions of measured suspended sediment fine with increasing distance from the bed. Additionally, the percentage of sediment finer than 15 μm measured in the suspended sediment samples increases with distance above the bed, from 5–10% near the bed to 50–60% near the surface (supporting information). At the Kenli reach, the Yellow River channel bed is remarkably smooth: Long-wavelength bedforms do little to disrupt or extract momentum from the flow yet create 2–5 m variation in flow depth along the survey reach (Ma et al., 2017).

3.3. Shear Velocity Calibration

Velocity profile data were not collected in the 2015 survey, and so a relationship for flow depth and shear velocity was initially substituted (i.e., depth-slope product, $u_* = \sqrt{gHS_0}$; Leopold et al., 1995). However, the only varying parameter in the depth-slope product calculations is the flow depth (H), and local variability in flow depth is poorly correlated to reach-averaged shear stress and suspended sediment concentration (e.g., Figure 6; Pearson correlation coefficient, $r = 0.34$; An et al., 2018).

In 2016 and 2018, water velocity profile measurements were made at each station with an acoustic Doppler current profiler (ADCP) and a mechanical propeller-driven velocimeter. Local shear velocity was determined from a resistance relation and measured depth-averaged velocity (Ma et al., 2022); measured depth-averaged velocity is derived from weighted ADCP and velocimeter measurements. To estimate shear velocity when no direct velocity measurements are available, we produce a calibration that relates water discharge data (Q_w, collected ~10 km upstream at a nearby gauging station operated by the Yellow River Hydrological Bureau) and the local flow depth (H), to predict reach-scale shear velocity. The shear velocity calibration is found by linear regression of log-transformed variables ($R^2 = 0.80$; supporting information) and rescaled to a power law relation (Figure 6):

$$u_{*,\mathrm{calib}} = 0.0202[Q_w]^{0.083}[H]^{0.298}, \tag{13}$$

where shear velocity, discharge, and depth have units of m/s, m^3/s, and m, respectively; Equation 13 is nonhomogeneous and depends on selected units. For consistency, this calibration is applied to determine the shear velocity for all survey stations. The effects of form drag on shear stress partitioning, including bedforms (McLean, 1991, 1992; McLean et al., 1994), are ignored in calibrating the shear velocity.

4. Measuring Adjustment to Velocity and Concentration Profiles

We compare three models for velocity and concentration throughout the text: (i) Equations 4–6 for $\alpha = 1$ yield a dilute suspension prediction (denoted by variables with subscript 1.0), (ii) Equations 4–6 for $\alpha = f(w_s/u_*, \bar{C}, S_0)$ yield an α-stratified prediction (where a subscript on α denotes a specific prediction or analytical approach; Equation 10), and (iii) a buoyancy-stratified model that assumes Reynolds-averaged turbulent characteristics are in local equilibrium (Mellor & Yamada, 1982; Yeh & Parker, 2013, denoted by variables with subscript MY).

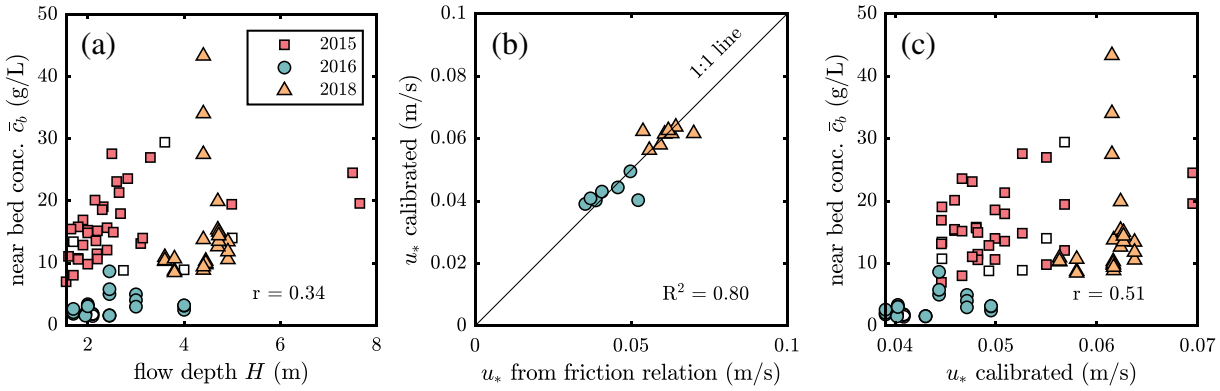

Figure 6. Calibration for shear velocity (u_*) for all measurements. (a) Near bed concentration is poorly correlated with the local flow depth (Pearson correlation coefficient, $r = 0.34$). (b) u_* derived from depth-averaged flow velocity and a resistance relation grounds a calibration (Equation 13) relating discharge measured at Lijin station and local flow depth to shear velocity. The calibration smooths local variations in depth that are not reflected in corresponding suspensions. (c) Improved correlation between shear velocity and near bed concentration (Pearson correlation coefficient, $r = 0.51$). Outliers are plotted as open symbols.

Concentration profile adjustment, which may be due to both density stratification and sediment diffusivity variability, was identified by comparing measured concentration profiles ($\bar{c}_f$) to predictions from a dilute-suspension model ($\bar{c}_{1.0}$). The measured sediment concentration profiles of each grain-size class ($\bar{c}_{f,i}$) were fit with Equation 5, where $\bar{c}_{b,i}$ and $Z_{Rf,i}$ are free parameters to account for concentration measurement uncertainty. The fit near-bed concentration (i.e., $\bar{c}_{b,i}$) is used as the reference concentration in subsequent analyses. Similarly, the cumulated sediment concentration for all grain-size classes was fit to produce a concentration profile ($\bar{c}_f$), where the bulk Rouse number (Z_{Rf}) is determined from the bed material median grain size (D_{50}; Figure 5a–5c). The measured near-bed grain-size distribution and concentration data were used to evaluate grain-size specific concentration profiles according to the (i) dilute-suspension ($\bar{c}_{1.0,i}$), (ii) α_{WP04}-stratified ($\bar{c}_{WP04,i}$), and (iii) buoyancy-stratified ($\bar{c}_{MY,i}$) models.

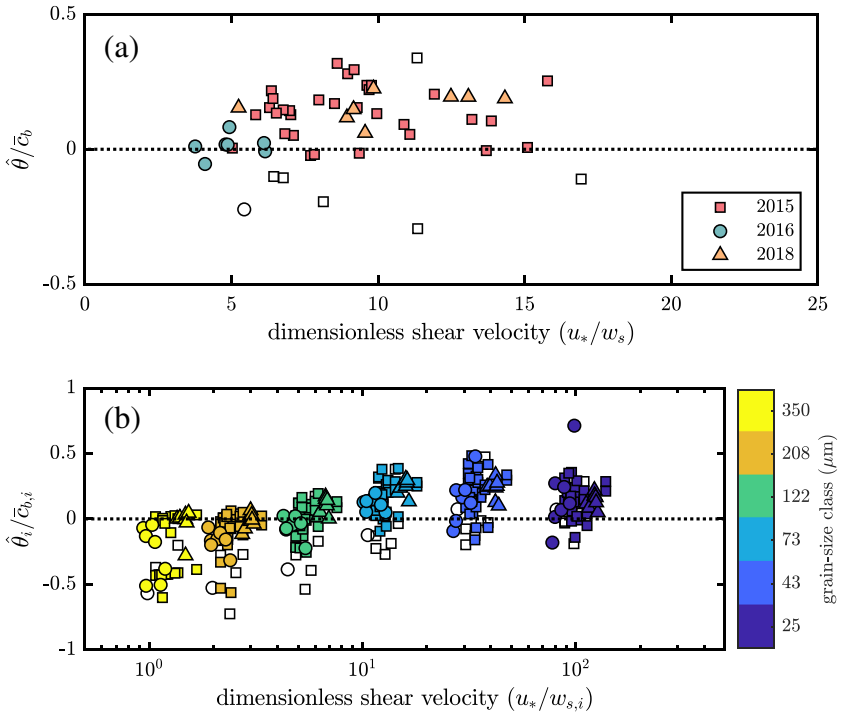

Figure 7. (a) Normalized mean signed deviation of $\bar{c}_{1.0}$ and $\bar{c}_f$ (Equation 14) as a function of dimensionless shear velocity. Differences in the profiles are apparent only in samples collected under larger dimensionless shear velocity conditions. (b) Grain-size-specific normalized mean signed deviation (Equation 14). Misprediction of the dilute-suspension models scales primarily with the grain-size class. Outliers are plotted as open symbols.

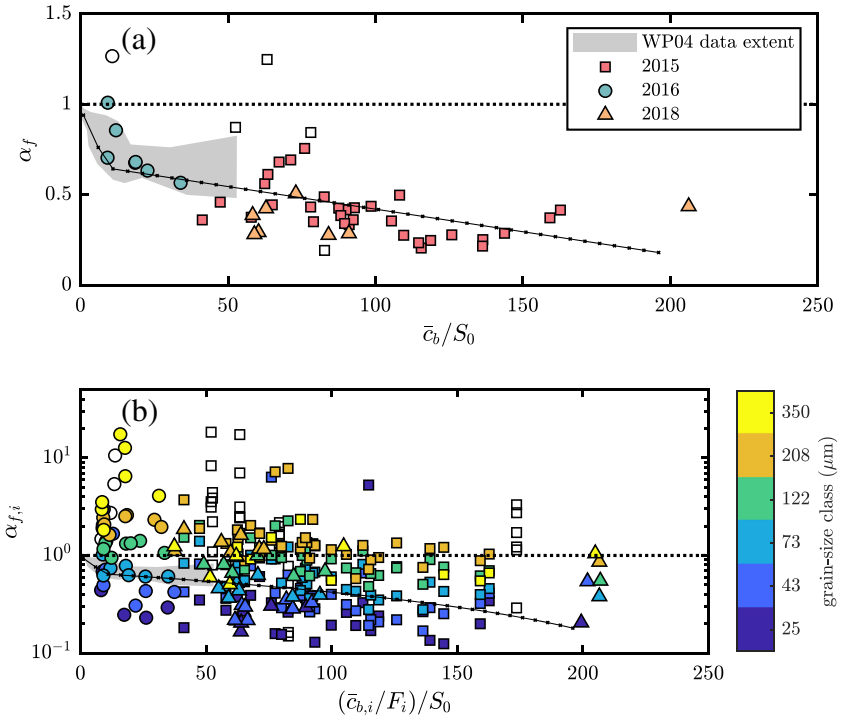

Figure 8. (a) α_f calculated by the ratio of the field measured Rouse number (Z_{Rf}) to Rouse number from the dilute-suspension model ($Z_{R1.0}$). (b) Grain-size specific $\alpha_{f,i}$. Outliers are plotted as open symbols.

The normalized mean signed deviation for grain size class i ($\hat{\theta}/\bar{c}_{b,i}$) between a dilute-suspension ($\bar{c}_{1.0,i}$) and best fit ($\bar{c}_{f,i}$) model pair was calculated as

$$\frac{\hat{\theta}_i}{\bar{c}_{b,i}} = \frac{\sum_{\hat{z}=1}^{l}[\bar{c}_{1.0,i}(\hat{z}) - \bar{c}_{f,i}(\hat{z})]/l}{\bar{c}_{b,i}}, \tag{14}$$

where $\hat{z}$ is a discrete mapping of vertical coordinate z and $l = 51$ is the number of points where the models are evaluated. Similarly, the mean signed deviation was calculated between a cumulated dilute-suspension ($\bar{c}_{1.0}$) and best fit ($\bar{c}_f$) model pair. This statistic characterizes the degree of error for the dilute-suspension model, where $\hat{\theta}/\bar{c}_b > 0$ implies an offset consistent with density stratification.

The mean signed deviation for the grain-size-cumulated dilute-suspension model is positive for all values of the dimensionless shear velocity (Figure 7a). There is a positive relationship between dimensionless shear velocity and normalized mean signed deviation for each grain-size class (note the symbol sequence, circle→square→triangle, for each grain-size class; Figure 7b). However, the grain-size specific normalized mean signed deviation scales predominantly with dimensionless shear velocity due to the different grain-size classes, rather than variable flow conditions. Specifically, $\hat{\theta}_i/\bar{c}_{b,i}$ increases with dimensionless shear velocity, from approximately zero for the coarsest grain-size class, but decreases in the smallest two grain-size classes (Figure 7b).

The adjustment coefficient in the Rouse number (Equation 6) necessary to produce a measured sediment concentration profile is given by $\alpha_{f,i} = Z_{Rf,i}/Z_{R1.0,i}$ for each grain-size class i, because α is assumed to be unity in the dilute-suspension model $\bar{c}_{1.0,i}$. The cumulated grain-size-measured concentration profile is contrasted with the Rouse number for the median bed material and compared to the prediction for α (Equation 10, Figure 8a; Wright & Parker, 2004b).

A larger adjustment to the concentration profile (decreasing α) occurs with increasing near-bed concentration-to-slope ratios (Figure 8a). The near-bed concentration-to-slope ratio is expected to scale density stratification, because it appears in the Richardson number (i.e., Equations 8 and 9). The Yellow River

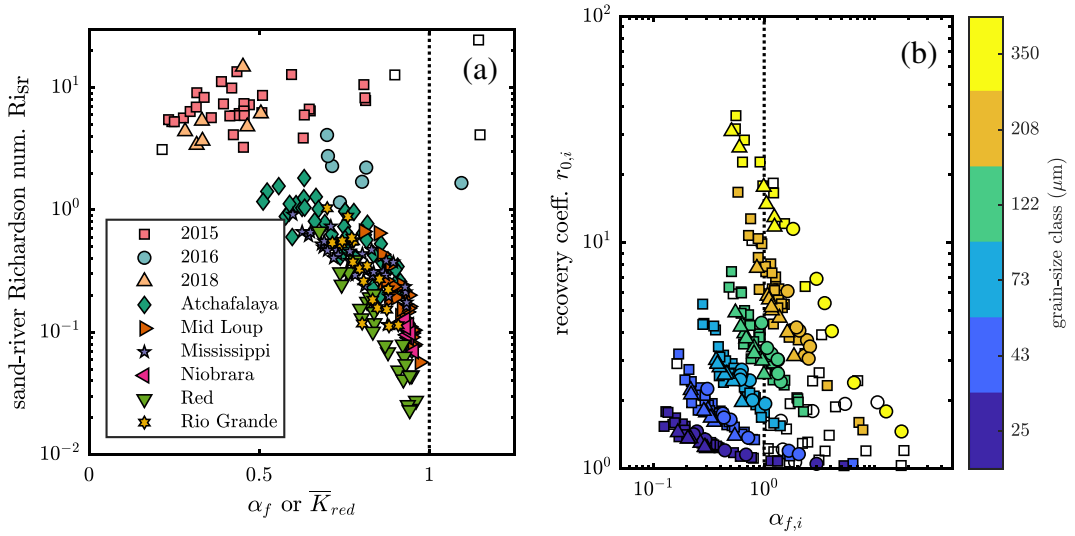

Figure 9. (a) Sand-river Richardson number (Equation 9) and (b) recovery coefficient (Equation 15) as a function of the depth-averaged reduction in eddy viscosity. Outliers are plotted as open symbols. The Yellow River data extend the range of stratification effects previously measured in the field. The recovery coefficient indicates that the behavior of sediment entrainment and deposition on the bed depends on grain size and stratification.

data provide much higher $\bar{c}_b/S_0$ ratios than previously measured in the field and coincide with the $\alpha_{WP\,04}$ prediction (Equation 10; Wright & Parker, 2004b). The grain-size-specific calculations show a similar trend, but the $\alpha_{f,i}$ coefficient for different grain-size classes decreases as the grain size decreases (Figure 8b): Smaller grains deviate from the dilute-suspension model more than larger grains, for the same $\bar{c}_b/S_0$ ratio. The grain-size specific stratification calculation is sensitive to poorly fitting concentration profiles of the coarsest and finest grain-size classes that arise from small sediment concentrations in these grain-size classes. For example, a very low concentration of sediment >208 μm yielded $\alpha_{f,i}$ values that are >10 (Figure 8b). Similarly, the finest grain-size class yielded spurious $\alpha_{f,i}$ values due to the minute concentration of fine sediment in suspension (recall that washload <15 μm was excluded from the calculations).

The $\alpha_{WP\,04}$ model consistently overpredicts the cumulative concentration profile, especially so in the upper portions of the water column (Figure 5; supporting information). This is because the $\alpha_{WP\,04}$ model applies the same α value to each grain-size class profile prediction, rather than an α value that reflects variable stratification of each class. Specifically, the cumulative concentration profiles are mismatched to the measured profiles due to the coarsest and finest grain-size classes.

Larger sand-river Richardson numbers correspond to increasing concentration profile adjustment (Figure 9a). Interestingly, the trend of the Wright and Parker (2004a) model for sand-bed rivers is extended by adding the Yellow River data. The shape of the concentration profile was characterized by the recovery coefficient (r_0):

$$r_0 = \bar{c}_b/\bar{C}, \tag{15}$$

where a value ≥1 is expected for open-channel flows, but this value varies considerably as a function of environmental parameters (Cao et al., 2006; Duan & Nanda, 2006; Zhang & Duan, 2011; Zhang et al., 2013). The recovery coefficient is useful for predicting the behavior of sediment entrainment and deposition on the bed in morphodynamic modeling (An et al., 2018; García, 2008). Each grain-size class shows an increase in the recovery coefficient with increasing stratification effects (decreasing $\alpha_{f,i}$). The r_0 values for the finest grain-size class are ≥1 (i.e., stratified) for all measured conditions. r_0 values for coarser grains-size classes (≥122 μm) increase approximately exponentially as a function of the density stratification increase, reaching an r_0 value of ~12 for the coarsest grain-size classes. Each grain-size class trends along a different power law relationship between recovery coefficient (r_0) and stratification ($\alpha_{f,i}$). Importantly, the recovery coefficient observations indicate that sediment entrainment and deposition behavior depends on stratification, in addition to well-known grain-size effects (e.g., An et al., 2018).

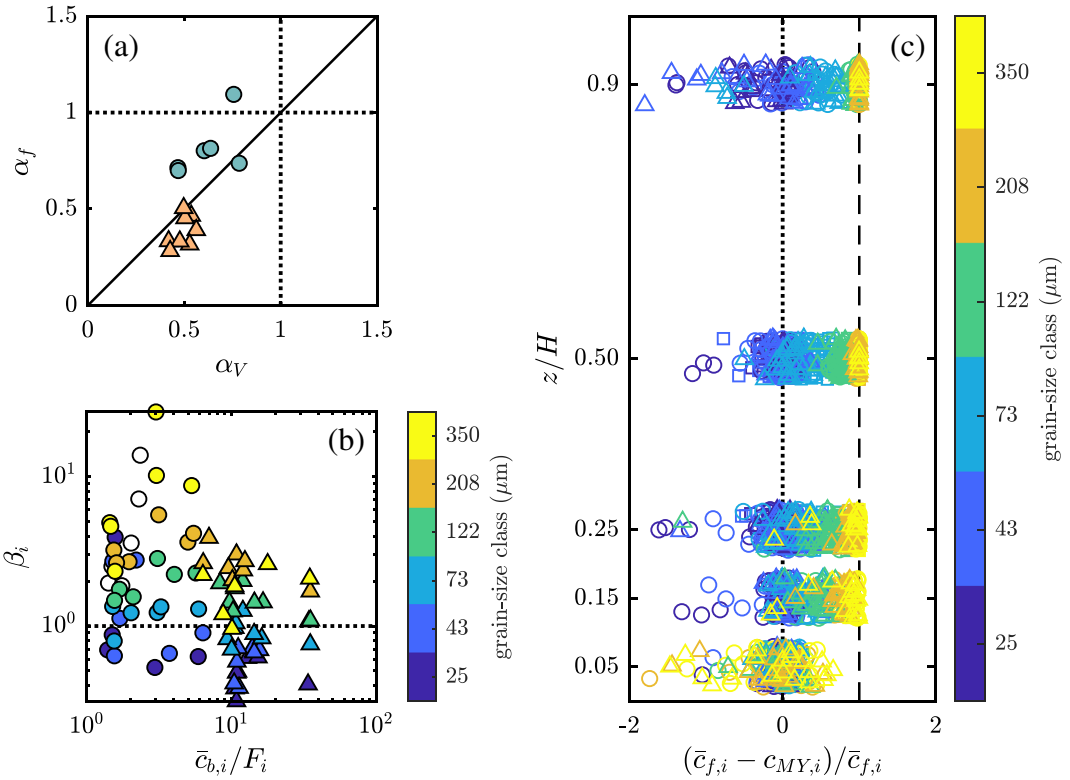

Figure 10. (a) Comparison plot of α_V determined from the fit to velocity profiles versus α_f fit to the concentration profiles. (b) β as a function of concentration; outliers are plotted as open symbols in this panel. (c) Ratio of measured sediment concentration over the concentration predicted by the buoyancy-stratified model.

4.1. Isolating Sediment Diffusivity Effects

The measured concentration profiles are also modulated by the sediment diffusivity coefficient (β), which describes the relationship between sediment and water transport in turbulent eddies. However, if the effects are assumed to interact linearly to modulate the Rouse number (i.e., if $Z_{R,i} = w_{s,i}/\beta\alpha_V\kappa u_*$), then the value of the sediment diffusivity coefficient (β) can be elucidated by comparing the α_f value derived from the sediment concentration profiles with an adjustment coefficient derived from the measured velocity profiles at the same station (α_V). Note that this is a functionally equivalent approach to the "apparent von Kármán number" κ_a from Einstein and Chien (1955), where $\kappa_a = \kappa\alpha_V$ (Wright & Parker, 2004b). α_V was determined by the slope of a best fit line to the velocity profile measurements in log-linear space while holding the shear velocity fixed (Figure 10a; supporting information). Additionally, the calculations herein using the buoyancy-stratified model assume a sediment diffusivity of $\beta = 1$, which enables a comparison between field data and modeled profiles to reveal the behavior of sediment diffusivity with respect to turbulence, as a function of grain size.

The stratification coefficients derived from the velocity and concentration profiles were approximately equal and near unity for the 2016 data, which show minimal density stratification ($\alpha_V \approx \alpha_f$; Figure 10a). Both profile adjustments are less than unity for 2018, when there was considerable density stratification. Interestingly, the adjustment to the concentration profile exceeds the adjustment to the velocity profile (Figure 10a).

The sediment diffusivity coefficient can be directly recovered from the velocity profile density stratification adjustment coefficient α_V, if the effects are assumed to interact linearly to modulate the Rouse number (i.e., if $Z_{R,i} = w_{s,i}/\beta\alpha_V\kappa u_*$). Under this assumption, $\beta = \alpha_f/\alpha_V$. The sediment diffusivity coefficient of each grain-size class decreases with increasing near-bed concentration (Figure 10b).

The buoyancy-stratified model calculations assume that the sediment diffusivity coefficient is equal to unity ($\beta = 1$); the mismatch between the measured and buoyancy-stratified concentrations thus quantifies the

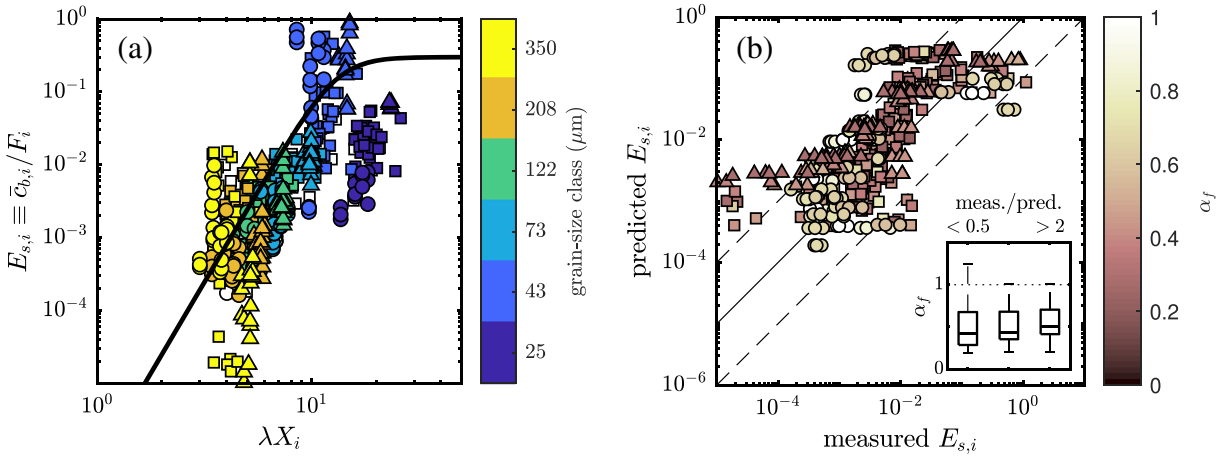

Figure 11. (a) Near-bed concentration as a function of the grain size sorting (λ) and entrainment parameter X_i. Black line is the prediction by Equation 12 (Wright & Parker, 2004b); outliers are plotted as open symbols in this panel. (b) Correlation between measured and predicted concentration (using Equation 12); outliers are omitted. Dashed lines represent 1 order of magnitude from the 1:1 line. (Inset) Boxplot of stratification effect α_f for $E_{s,i}$ measurements, grouped by the factor by which the measured exceeds the predicted (axis label above inset). Symbols are the same as in Figure 7.

actual sediment diffusivity behavior in the flow. The normalized error of the buoyancy-stratified profile with respect to the measured samples is calculated for each grain-size class ($(\bar{c}_{f,i} - c_{MY,i})/\bar{c}_{f,i}$) and examined as a function of distance above the bed (Figure 10c). A normalized error value of zero indicates that the buoyancy-stratified model matches the measurement, a normalized error value <0 implies sediment inertia leads to diffusivity less than the fluid eddy diffusivity ($\beta < 1$), and a fractional-error value >0 implies momentum carries sediment beyond fluid eddies ($\beta > 1$).

There is an overall increase in the variability of the normalized error metric (positive and negative) with increasing distance above the bed (Figure 10c). Additionally, the finer grain sizes tend slightly toward negative normalized error values, whereas the coarser grain-size classes tend toward the upper limit value of 1 (Figure 10c). Note that the buoyancy-stratified model uses the field-measured near-bed concentration and grain-size distribution as boundary conditions. The prediction thus matches the data measured near the channel bed due to proximity to the boundary. The precise normalized error value should be interpreted with caution, because the metric has an upper bound at unity and is sensitive to low concentrations predicted from the buoyancy-stratified model.

4.2. Sediment Entrainment Impacted by Stratification

The entrainment parameter X_i (Equation 12) is calculated for each grain-size class i of the near-bed suspended sediment samples and plotted against the measured concentrations, where $E_s = \bar{c}_{b,i}/F_i$ (Figure 11a). The Yellow River data generally agree with the Wright and Parker (2004b) prediction (Equation 11): The prediction exceeds the measured value for the finer grain-size classes (≤73 μm), but most measurements are within an order of magnitude of the predicted value. The largest and smallest grain-size classes show the largest deviation from the prediction (Figure 11a). In particular, $E_{s,i}$ of the smallest grain-size class (25 μm) extends several orders of magnitude below prediction, and the second-smallest class (43 μm) $E_{s,i}$ exceeds the theoretical concentration limit of a fluid of 0.3 (recall that $E_{s,i}$ is a distribution-normalized measured concentration and not the true measured concentration Turner, 1979).

On visual inspection of Figure 11a, it appears that the entrainment rates for samples collected in 2016 (circles, minor stratification effects) exceed or match prediction, whereas the entrainment rate for samples collected in 2018 (triangles, significant stratification) fall below prediction. This observation is quantified by the inset boxplots in Figure 11b. The median α_f is 0.51 when the measured concentration exceeds the predicted value by a factor of 2 (meas./pred. > 2), whereas the median α_f is 0.42 when the measurement was less than half of the prediction (meas./pred. < 0.5). These sample groups are statistically different, as determined by a Wilcoxon rank sum test ($p = 8.5 \times 10^{-3}$).

5. Discussion

5.1. Density Stratification and Sediment Diffusivity

Direct measures of sediment-induced density stratification, both in laboratory and field settings, are limited. The normalized mean signed deviation and α_f statistics (Figures 7 and 8) confirm the presence of modulated concentration profiles in the Yellow River, particularly at high sediment concentration. Furthermore, the grain-size specific calculations of the mean signed deviation and $\alpha_{f,i}$ show that sediment grain size is not uniformly stratified.

However, the patterns of concentration profiles adjustment documented herein (as α_f and $\alpha_{f,i}$) are confounded by density stratification and sediment diffusivity variability, which also varies according to grain size and concentration. It is difficult to isolate these effects in natural flows, because sediment concentration and density stratification evolve nonlinearly with increasing shear stress (Winterwerp, 2006). However, experimental studies have quantified sediment diffusivity coefficients in dilute suspension conditions and concluded that β is predominately a function of grain size (Graf & Cellino, 2002; Rose & Thorne, 2001; van Rijn, 1984). Observations from the Yellow River confirm a grain-size dependence of sediment diffusivity (Figure 10b), as well as a dependence on concentration. A decrease in β with increasing concentration is consistent with observations of grain-grain collisions in the flow (Nezu & Azuma, 2004). Grain-size classes $\geq$122 μm consistently have positive normalized error values, and finer grain-size classes typically have negative normalized error values, as characterized by sediment diffusivity coefficient $\beta > 1$ for coarse sediments and $\beta \leq 1$ for fine sediment (e.g., Figure 10c, van Rijn, 1984).

There is controversy surrounding the variability of β with distance above the bed. Rose and Thorne (2001) demonstrated β is independent of distance above the bed, yet Bennett et al. (1998) identified a pattern of variation of β with distance above the bed. Unfortunately, comparison of Rouse numbers (Figures 10a and 10b) and boundary conditions of the buoyancy-stratified model ($\bar{c}_{MY}$; Figure 10c) preclude elucidating depth dependence in the Yellow River data. Buoyancy-stratified calculations using the Mellor and Yamada (1982) model and river concentration profiles, which allow a flexible boundary condition, may help to inform about sediment diffusivity behavior.

The variability in the behavior of sediment diffusivity has a net-zero effect on the adjustment coefficient (α_f) of the cumulative concentration profile, as seen by the agreement with the Wright and Parker (2004b) prediction (Figure 8a; Equation 10). However, grain-size specific profile adjustments scatter around the $\alpha_{WP\,04}$ prediction (Figure 8b), likely because the $\alpha_{WP\,04}$ prediction is calibrated by modeling that assumes $\beta = 1$. Cumulative concentration profile alignment with the $\alpha_{WP\,04}$ prediction, despite grain-size specific variation, suggests that sediment diffusivity variability is a second-order control on the shape of the concentration profile, modulating grain-size specific concentration profiles, but not in any meaningful way when the profiles are cumulated.

Density stratification is the primary control on the adjustment coefficient. There is a large change in α_f as concentration changes, and suspended grain size is relatively fixed (Figures 5g–5i and 8a). It might be expected that with increasing stress, a given grain size is more uniformly distributed. However, the trends in r_0 indicate that turbulence suppression due to density stratification overwhelms the concomitant increase in the u_*/w_s ratio; near-bed concentration increases significantly with increasing shear stress, but sediment is not distributed to the entire water column because turbulent mixing is inhibited. Thus, despite sediment diffusivity variability modulating grain-size specific concentration profiles, stratification is the primary control on profile shape and magnitude. Nevertheless, as a value of α greater than unity has no reasonable physical meaning (Wright & Parker, 2004a), α_f and $\alpha_{f,i}$ values greater than 1 are likely influenced by variable sediment diffusivity effects. Thus, when concentration is sufficiently low that stratification effects are minimal (i.e., the 2016 survey), the dominant control on profile shape is grain-size specific sediment diffusivity (Figures 8b and 10b).

5.2. Sediment Entrainment

Entrainment relations seek to link flow and bed material properties to predict near-bed sediment concentration. Generally, the measured Yellow River sediment concentrations agree with the trend of the Wright and Parker (2004b) model (Equation 11) across grain-size classes, barring the largest and smallest grain-size classes (Figure 11a).

The increased variability of the largest grain-size class could be due to the distribution-normalizing procedure used to determine $E_{s,i}$. Alternatively, increasing sediment diffusivity of coarse grain sizes leads to higher than expected near-bed concentration, although this would be inconsistent with the physical interpretation that increased sediment diffusivity requires particles be elevated from the bed by decaying turbulent eddies. Otherwise, larger variability in the instantaneous near-bed concentration may be due to the larger grain sizes concentrated there (Gitto et al., 2017).

The sediment entrainment rate of the finest grain-size class is approximately 2 orders of magnitude lower than predicted (Figure 11a). This is not a consequence of the treatment of washload sediment (<15 μm), because F_i in the distribution-normalizing procedure to determine $E_{s,i}$ is the fraction of the washload-free suspended sediment samples. Instead, the lower than predicted entrainment is interpreted to result from sediment supply limitation in this grain-size class—consistent with the expectation for sediment found in limited quantity on the bed. However, the sediment concentration in this class is positively correlated with λX_i, implying that sediment is indeed sourced from the bed. The implications of these observations are discussed in further detail in the following section.

Variability in entrainment is correlated with density stratification (Figure 11b). Specifically, the samples collected in a flow with weaker density stratification show higher entrainment rates than predicted, whereas stratified flows reduce entrainment rates. This supports the notion that suppressed turbulence due to density stratification lowers entrainment (Vanoni, 1941).

5.3. Grain-Size-Specific Effects of Stratification and Defining Washload

There are varying definitions of washload (Woo et al., 1986), such as a combination of criteria including (1) proportionally small quantities on the channel bed, (2) supply limitation, (3) a Rouse number suggesting uniform concentration (Hill et al., 2017), (4) finer than a defined grain-size threshold (Partheniades, 1977), or (5) lack of contribution to change in channel-bed slope (Paola et al., 1999). In the Yellow River, fine sediment displays unexpected and interesting behavior that deviates from coarser grain-size classes (e.g., Figures 8b, 9b, and 11a). Specifically, the entrainment observations provide contradictory evidence for supply- and transport-limited sediment transport (Figure 11a), and the recovery coefficient (r_0) indicates that the finest grain-size class is nonuniformly distributed and stratified, which questions the appropriate definition of washload for this system. Interestingly, stratified very fine sediment may indicate that this sediment is flocculated while in transport (Lamb et al., 2020). A supply-limited finest grain-size class implies that the washload threshold used in this study (15 μm) is too fine, whereas nonuniform vertical distribution and stratification of the finest grain-size class suggest that the washload threshold may be too coarse.

The fifth percentile grain size of the cumulative channel bed grain-size distribution has been recognized to demarcate the threshold to washload (e.g., Woo et al., 1986). Based on this criterion, the Yellow River washload threshold would be 40–50 μm (Figure 5g–5i). However, the upper extent of supply limitation observed in entrainment measurements is between 25 and 43 μm (Figure 11a). The finest grain-size class has extremely small Rouse numbers (Figure 8b), yet this sediment contributes to energy dissipation and is not uniformly distributed in the flow (Figure 9b). Taken together, the observations are most consistent with a washload definition that incorporates a dimensionless shear velocity (e.g., a Rouse number; Equation 6; Hill et al., 2017). These observations underscore the importance of establishing a washload cutoff based on the research question of interest: It is necessary to consider even the finest sediment to study the turbulent energy budget for a flow, yet a definition that considers material comprising the bed is appropriate for morphodynamic modeling, as this considers only material that affects the transport capacity of the flow (Dong et al., 2019; Li et al., 2015; Paola et al., 1999). This highlights the need to reexamine the behavior of fine sediment in open channel flows (Lamb et al., 2020).

5.4. Adjustment to Rouse Profiles

The $\alpha_{WP\,04}$ model (Equation 10) overestimates the concentration in the upper half of the water column (Figures 5a–5c; supporting information) because the $\alpha_{WP\,04}$ model ignores grain-size-specific variability in stratification effects (i.e., applies the same adjustment to each concentration profile). To address the grain-size-dependent variability in stratification conditions, a modified prediction is proposed. The $\bar{c}_b/S_0$ ratio correlates strongly with bulk density stratification effects, and this ratio offers an independent variable in the $\alpha_{WP\,04}$ relation (Equation 10) but precludes grain-size-specific stratification effects. The data from this

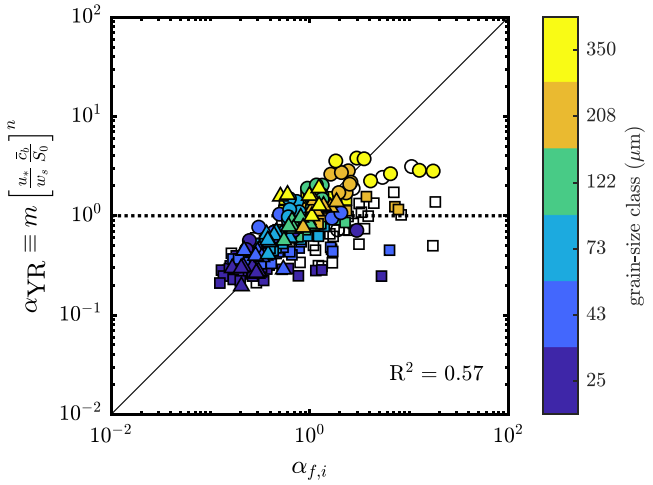

Figure 12. Correlation between grain-size-specific $\alpha_{f,i}$ and predicted concentration profile adjustment from Equation 16. Outliers are plotted as open symbols.

study are recast in terms of a multivariate linear regression, whereby the eddy viscosity adjustment coefficient ($\alpha_{f,i}$) is dependent on the sand-river Richardson number (Equation 9; Figure 12). The regression equation obtained (omitting outliers) is

$$\alpha_{\mathrm{YR,i}} = m\left[\frac{u_*}{w_{s,i}}\frac{\bar{c}_b}{S_0}\right]^n, \tag{16}$$

where $m = 8.2$ and $n = -0.37$ ($R^2 = 0.57$). The finest and coarsest grain-size classes are omitted from the regression, because they often have extreme values. Nevertheless, these data plot along the same trend as the center-distribution grain-size classes (Figure 12). The relation predicts the *total* adjustment to the concentration profile and so includes density stratification and sediment diffusivity variability. The formulation depicts the distribution of energy balance specifically in the case of the Yellow River and should therefore be applied cautiously to other rivers.

The bulk stratification coefficient remains a useful metric in other rivers, but observed stratification is poorly explained by existing relations ($R^2 = 0.15$ for Equation 10). Therefore, we introduce a relation incorporating grain size, concentration, and slope, which uses auxiliary variables o and p for a given slope:

$$\alpha_{S_0} = 1 - \left[o\left(\bar{c}_b \mathrm{Re}_{\mathrm{p},50}^{-0.6}\right)^p\right], \tag{17}$$

where $o = 0.025(\log_{10}S_0) + 3.20$ and $p = 0.11(\log_{10}S_0) + 0.79$ and $\mathrm{Re}_{\mathrm{p},50}$ is the particle Reynolds number of the median grain size of bed material ($R^2 = 0.33$; Figure 13). For the purposes of this regression, the data from Wright and Parker (2004a, 2004b) are treated as field-validated data. Our new predictive relation requires an additional input, though specification of this input (particle Reynolds number $\mathrm{Re}_{\mathrm{p},50}$) depends only on median grain size and environmental constants (ν and g), which we expect to be known in most applications. A larger data set of concentration profiles from global rivers is likely to improve predictions (de Leeuw et al., 2020).

Calculations were performed with the buoyancy-stratified model, using a global data set of river properties as the boundary condition (Li et al., 2015); the sediment mixture is assumed to be single size, and entrainment follows Equation 11 (Wright & Parker, 2004b). This set of calculations follows similar trends to the separation identified by α_{S_0} (Equation 17). Additional $\bar{c}_{MY}$ calculations are randomly sampled from the parameter space of the data set of global rivers from Li et al. (2015), and the depth-averaged eddy viscosity

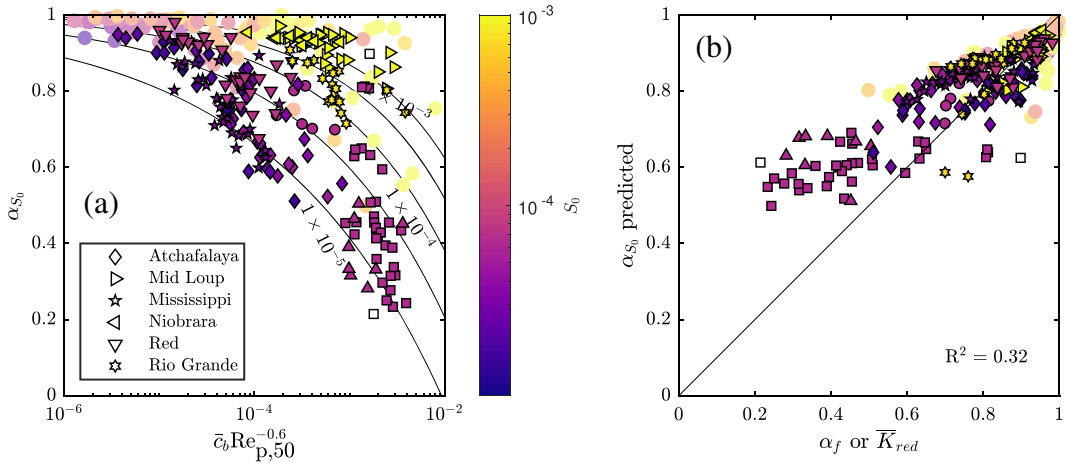

Figure 13. (a) Depth-averaged reduction in eddy viscosity as a function of near-bed concentration and particle Reynolds number. Rivers separate along contours of channel-bed slope. (b) Correlation between measured and predicted α by Equation 17. Outliers are plotted as open symbols.

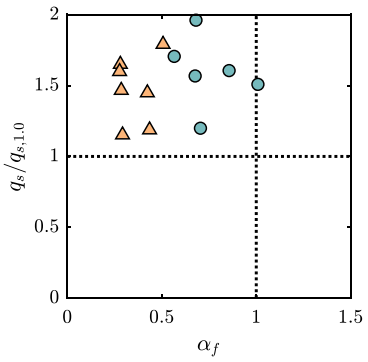

Figure 14. Ratio of depth-discharge-integrated sediment transport (Equation 1) under density-stratified flow to predicted transport assuming a dilute suspension ($\alpha = 1$ in Equations 4 and 5).

is never reduced below $\tilde{K}_{red} = 0.25$ (supporting information). This is consistent with the Yellow River measurements, where $\alpha_f \approx 0.2$ was the minimum value. This may represent a physical limit to the reduction of the eddy viscosity profile and could inform turbulent energy budgets of other river systems. Alternatively, this may be a numerical artifact relating to extinguished turbulence (e.g., Wright & Parker, 2004a). An area of focus for future work is to systematically explore this lower limit, by manipulating suspension properties like grain size, slope, and concentration.

5.5. Predicting Sediment Transport

The suspended sediment flux in a river is impacted by density stratification (Vanoni, 1941, 1946; Wright & Parker, 2004a). Depth-discharge-integrated sediment flux (i.e., Equation 1) measured in the Yellow River is greater than predicted by dilute-suspension log-law velocity and Rouse concentration profiles ($\alpha = 1$, Equations 4–6; Figure 14a). Enhanced sediment transport is opposite from the model results of Wright and Parker (2004a). Enhanced transport may be due to lower flow resistance in the Yellow River than other large low-sloping rivers (Ma et al., 2017, 2022), whereby flow acceleration offsets reduced concentration, so as to maintain net increase in sediment transport rate. Predicting the depth-averaged density stratification coefficient α (e.g., by Equation 16) and applying the adjusted log-law velocity and Rouse concentration profiles improves sediment flux calculations with respect to measurements. However, more velocity and concentration profile data are needed for a wide range of rivers to provide further validation of net sediment transport modulation due to density stratification.

Density stratification reduces sediment concentration in the upper portion of the water column and, when combined with sediment diffusivity variability, modulates the grain-size distribution. This is important because engineered sediment diversions typically off-take the upper portion of flow (e.g., Nittrouer & Viparelli, 2014), yet, to maximize coarse material flux, should draw water from the lower region of flow, where coarse material is focused. In the Yellow River, the grain-size distribution in the upper 20% of the flow is finer than predicted by the dilute-suspension model (validated by Wilcoxon signed rank test; supporting information), and the overall sediment concentration is reduced by 1–20% (supporting information). Interestingly, the concentrations of the coarsest grain-size classes (≥208 μm) are increased relative to the dilute-suspension prediction in the upper water column (supporting information). In contrast, concentrations of medial grain sizes (73–208 μm, which comprise most of the grain-size distribution) are reduced relative to the prediction, and the finest grain-size class concentrations (<73 μm) are relatively unaffected (supporting information). Taken together, grain-size-specific concentration profile adjustments indicate that the increase in the coarsest grain-size classes, in conjunction with accelerated flow velocity, leads to the net increase in suspended sediment flux due to stratification. The increase in coarse sediment in the upper water column is unexpected, and additional research is needed to verify this outcome and determine its cause.

The buoyancy stratified model of Mellor and Yamada (1982) accurately predicts the cumulative grain-size concentration profiles across the full range of observed density stratification (supporting information). The stratification conditions documented in this study are among the strongest observed in any natural open-channel flow, which means that the buoyancy-stratified model is likely accurate for other flow and sediment-mixture conditions. While the Mellor and Yamada (1982) model is analytically complex, software packages provide a simple method to predict suspension conditions (e.g., Yeh & Parker, 2013). These packages should be widely adopted when designing sediment diversion structures, because projects targeting large low-sloping rivers are prone to density stratification effects (Wright & Parker, 2004a, 2004b).

6. Conclusions

Despite a multitude of models predicting sediment transport dynamics in an open-channel flow, previous studies lacked the data necessary to robustly validate the effects of density stratification and sediment diffusivity over a range of natural river conditions. Larger density stratification effects are found in suspended

sediment concentration profiles in the Yellow River, than had been previously documented in natural river flows ($\alpha < 0.5$). Moreover, density stratification effects progressively developed with increasing river shear velocity, suggesting that while near-bed concentration increases significantly with increasing shear stress, a net turbulence suppression persists due to stratification, and so sediment is not distributed to the entire water column as predicted by clear-water concentration profile models. The density stratification effect is enhanced for fine sediment relative to coarse sediment, whereby the coarsest sediment is relatively unaffected. Fine sediment suspended in the river appears to be supply limited and is only sparsely present on the channel bed, yet this material is not uniformly distributed in the vertical and changes concentration with increasing shear stress. This suggests that even very fine sediment extracts turbulent energy from the flow and that the washload threshold grain size in the Yellow River is fine (<25 μm). Together, these findings indicate that modeling suspension grain size and concentration profiles requires accounting for density stratification effects, which may be achieved by application of the Mellor and Yamada (1982) model as detailed by Yeh and Parker (2013).

Additionally, measured concentration profiles are modulated by grain-size-specific sediment diffusivity, whereby variation in the sediment diffusivity significantly impacts the vertical distribution of sediment grain size at low sediment concentration. The sediment diffusivity documented in the Yellow river is consistent with a momentum effect for coarser sediment ($\beta > 1$), and a lagging inertial effect impacts finer sediment. Sediment entrainment is correlated with density stratification, whereby entrainment is reduced by suppressed turbulence near the bed in stratified flow. However, the overall entrainment rates observed are very similar to the Wright and Parker (2004b) relation.

In gross, observations of density stratification in the Yellow River indicate that river concentration profile modeling should include stratification effects, especially when predicting concentration and grain-size distribution near the surface of the water column, as in sediment diversion studies. Herein, formulations predicting a coefficient to adjust velocity and concentration profiles are presented for the Yellow River system and a more generally applicable model for rivers globally. Additionally, observations herein validate the Mellor and Yamada (1982) model over a range of stratification conditions, indicating that this model may be applied widely.

Notation

Symbol	Definition	Dimensions
b	bedload layer thickness	L
B	entrainment coefficient (Wright & Parker, 2004b)	—
$\bar{c}$	sediment concentration*	$\mathrm{M\,L^{-3}}$/—
$\bar{c}_b$	near-bed sediment concentration*	$\mathrm{M\,L^{-3}}$/—
$\bar{C}$	discharge weighted depth-averaged sediment concentration*	$\mathrm{M\,L^{-3}}$/—
D	grain size	L
D_{50}	50th percentile (median) grain size	L
D_{90}	90th percentile grain size	L
D_r	sediment deposition rate	$\mathrm{L\,T^{-1}}$
E_r	sediment entrainment rate	$\mathrm{L\,T^{-1}}$
E_s	dimensionless sediment entrainment rate	—
$\bar{F}_z$	net vertical sediment flux	$\mathrm{L\,T^{-1}}$
F_i	fraction of grain-size distribution in class i	
g	gravitational acceleration	$\mathrm{L\,T^{-2}}$
H	flow depth	L
i	grain-size class	—
k_s	flow roughness height	L
K_{m0}	clear-water eddy viscosity	$\mathrm{L^2\,T^{-1}}$
K_m	sediment-laden eddy viscosity	$\mathrm{L^2\,T^{-1}}$
K_{red}	depth-averaged reduction in eddy viscosity	—

Symbol	Definition	Dimensions
K_s	sediment diffusivity	$L^2\ T^{-1}$
m, n, o, p	regression coefficients	—
MY	relating to Mellor and Yamada (1982)	—
l	number of discrete intervals along $\hat{z}$	—
q_s	width-averaged sediment transport	$L^2\ T^{-1}$
Q_w	river water discharge	$L^3\ T^{-1}$
r_0	recovery coefficient	—
R	submerged specific gravity of sediment	—
Re_{pi}	particle Reynolds number of grain size i	—
Ri	Richardson number	—
S_0	channel/water surface slope	—
$\bar{u}$	streamwise flow velocity*	$L\ T^{-1}$
u_*	shear velocity	$L\ T^{-1}$
$u_{*,sk}$	skin-friction shear velocity	$L\ T^{-1}$
$\overline{w'c'}$	turbulent vertical flux of sediment*	$L\ T^{-1}$
w_s	particle settling velocity	$L\ T^{-1}$
WP04	relating to Wright and Parker (2004b)	—
X_i	entrainment parameter (Wright & Parker, 2004b)	—
z	quasi-vertical coordinate	L
$\hat{z}$	discrete coordinate along z	L
z_0	reference height	L
Z_R	Rouse suspension number	—
Z_{Rf}	best fit Rouse suspension number	—
Z_{Rp}	predicted Rouse suspension number	—
1.0	relating to modeled profile with stratification coefficient $\alpha = 1$	

*Overbar indicates averaging over turbulence.

Symbol	Definition	Dimensions
α	density stratification adjustment coefficient	—
α_f	field-measured (i.e., empirically fit) α from concentration profile	—
$\alpha_{1.0}$	modeled concentration profile when coefficient $\alpha = 1$	—
α_V	field-measured (i.e., empirically fit) α from velocity profile	—
α_{WP04}	predicted α via Equation 10	—
β	sediment diffusivity coefficient	—
γ	combined adjustment coefficient	—
$\hat{\theta}$	mean signed deviation†	—
κ	von Kármán constant	—
λ	grain-size sorting parameter	L
ν	kinematic viscosity	$L^2\ T^{-1}$
ρ	fluid density	$M\ L^{-3}$
ρ_s	sediment density	$M\ L^{-3}$
ϕ	Krumbein grain size scale	L
σ_ϕ	std. dev. of grain-size distribution in ϕ	L
τ_b	boundary shear stress	$M\ L^{-1}T^{-2}$
τ_{cr}	critical stress of mobility	$M\ L^{-1}T^{-2}$

†Retains units of test variable.

Data Availability Statement

The data, and processing and analysis code, are made available online. Processed and raw data sets can be found at Zenodo (https://zenodo.org/record/3457639). The processing scripts and plotting can be found at https://github.com/amoodie/paper_resources/ under `Moodie_densitystratification`.

Acknowledgments
A. J. M., J. A. N., H. M., B. N. C., M. P. L., and G. P. acknowledge support from the National Science Foundation (NSF) EAR-1427262 Coastal SEES grant. A. J. M. was supported by a NSF Graduate Research Fellowship under Grant No. 1842494 and a Geological Society of America Student Research grant. We are grateful to Kyle Strom and anonymous reviewers who contributed to improving the quality and clarity of this manuscript.

References

Amoudry, L. (2005). Schmidt number and near-bed boundary condition effects on a two-phase dilute sediment transport model. *Journal of Geophysical Research*, *110*, C09003. https://doi.org/10.1029/2004JC002798

An, C., Moodie, A. J., Ma, H., Fu, X., Zhang, Y., Naito, K., & Parker, G. (2018). Morphodynamic model of lower Yellow River: Flux or entrainment form for sediment mass conservation? *Earth Surface Dynamics*, *6*(4), 989–1010. https://doi.org/10.5194/esurf-6-989-2018

Anderson, A. G. (1942). Distribution of suspended sediment in a natural stream. *Transactions, American Geophysical Union*, *23*(2), 678. https://doi.org/10.1029/TR023i002p00678

Barton, J., & Lin, P. (1955). *A study of the sediment transport in alluvial channels*. Fort Collins, CO: Colorado A and M College, Civil Engineering Department.

Bennett, S. J., Bridge, J. S., & Best, J. L. (1998). Fluid and sediment dynamics of upper stage plane beds. *Journal of Geophysical Research*, *103*(C1), 1239–1274. https://doi.org/10.1029/97JC02764

Bolla Pittaluga, M. (2011). Stratification effects on flow and bed topography in straight and curved erodible streams. *Journal of Geophysical Research*, *116*, F03026. https://doi.org/10.1029/2011JF001979

Cao, Z., Pender, G., & Carling, P. (2006). Shallow water hydrodynamic models for hyperconcentrated sediment-laden floods over erodible bed. *Advances in Water Resources*, *29*(4), 546–557. https://doi.org/10.1016/j.advwatres.2005.06.011

Cellino, M., & Graf, W. H. (1999). Sediment-laden flow in open-channels under noncapacity and capacity conditions. *Journal of Hydraulic Engineering*, *125*(5), 455–462. https://doi.org/10.1061/(asce)0733-9429(1999)125:5(455)

Chan-Braun, C., Garcia-Villalba, M., & Uhlmann, M. (2010). *Numerical simulation of fully resolved particles in rough-wall turbulent open channel flow*. International Conference on Multiphase Flow 2010, University of Florida, Tampa, FL.

Colby, B. R. (1964). Discharge of sands and mean-velocity relationships in sand-bed streams (Tech. Rep. No): Geological survey professional paper 462-a.

Colby, B. R., & Hembree, C. H. (1955). Computations of total sediment discharge Niobrara River near Cody, Nebraska (Tech. Rep. No.). Geological survey water-supply paper 1357.

Coleman, N. L. (1970). Flume studies of the sediment transfer coefficient. *Water Resources Research*, *6*(3), 801–809. https://doi.org/10.1029/WR006i003p00801

de Leeuw, J., Lamb, M. P., Parker, G., Moodie, A. J., Haught, D., Venditti, J. G., & Nittrouer, J. A. (2020). Entrainment and suspension of sand and gravel. *Earth Surface Dynamics*, *8*, 485–504. https://doi.org/10.5194/esurf-8-485-2020

Dietrich, W. E. (1982). Settling velocity of natural particles. *Water Resources Research*, *18*(6), 1615–1626. https://doi.org/10.1029/WR018i006p01615

Dong, T. Y., Nittrouer, J. A., Czapiga, M. J., Ma, H., McElroy, B., Il'icheva, E., et al. (2019). Roles of bank material in setting bankfull hydraulic geometry as informed by the Selenga River Delta, Russia. *Water Resources Research*, *55*, 827–846. https://doi.org/10.1029/2017WR021985

Doshi, M. R., & Gill, W. N. (1970). A note on the mixing length theory of turbulent flow. *AIChE Journal*, *16*(5), 885–888. https://doi.org/10.1002/aic.690160532

Duan, J. G., & Nanda, S. (2006). Two-dimensional depth-averaged model simulation of suspended sediment concentration distribution in a groyne field. *Journal of Hydrology*, *327*(3–4), 426–437. https://doi.org/10.1016/j.jhydrol.2005.11.055

Einstein, H., & Chien, N. (1955). Effects of heavy sediment concentration near the bed on velocity and sediment distribution. U.S. Army Engineer Division, Missouri River.

Fildani, A., Normark, W. R., Kostic, S., & Parker, G. (2006). Channel formation by flow stripping: Large-scale scour features along the Monterey east channel and their relation to sediment waves. *Sedimentology*, *53*(6), 1265–1287. https://doi.org/10.1111/j.1365-3091.2006.00812.x

Galperin, B., Kantha, L. H., Hassid, S., & Rosati, A. (1988). A quasi-equilibrium turbulent energy model for geophysical flows. *Journal of the Atmospheric Sciences*, *45*(1), 55–62. https://doi.org/10.1175/1520-0469(1988)045<0055:AQETEM>2.0.CO;2

Ganti, V., Chu, Z., Lamb, M. P., Nittrouer, J. A., & Parker, G. (2014). Testing morphodynamic controls on the location and frequency of river avulsions on fans versus deltas: Huanghe (Yellow River), China: Avulsion drivers on fans versus deltas. *Geophysical Research Letters*, *41*, 7882–7890. https://doi.org/10.1002/2014GL061918

García, M. H. (2008). Ch 2: Sediment transport and morphodynamics, *Sedimentation engineering processes, measurements, modeling, and practice* (pp. 21–163). Reston, VA: American Society of Civil Engineers.

García, M., & Parker, G. (1991). Entrainment of bed sediment into suspension. *Journal of Hydraulic Engineering*, *117*(4), 414–435. https://doi.org/10.1061/(ASCE)0733-9429(1991)117:4(414)

García, M., & Parker, G. (1993). Experiments on the entrainment of sediment into suspension by a dense bottom current. *Journal of Geophysical Research*, *98*(C3), 4793–4807. https://doi.org/10.1029/92JC02404

Gelfenbaum, G., & Smith, J. D. (1986). Experimental evaluation of a generalized suspended-sediment transport theory. *Shelf sands and sandstones - Memoir 11* (pp. 339). Calgary, Alberta, CA: Canadian Society of Petroleum Geologists.

Ghoshal, K., & Pal, D. (2014). Grain-size distribution in suspension over a sand-gravel bed in open channel flow. *International Journal of Sediment Research*, *29*(2), 184–194. https://doi.org/10.1016/S1001-6279(14)60035-4

Gitto, A. B., Venditti, J. G., Kostaschuk, R., & Church, M. (2017). Representative point-integrated suspended sediment sampling in rivers: Representative sediment sampling. *Water Resources Research*, *53*, 2956–2971. https://doi.org/10.1002/2016WR019187

Graf, W. H., & Cellino, M. (2002). Suspension flows in open channels; experimental study. *Journal of Hydraulic Research*, *40*(4), 435–447. https://doi.org/10.1080/00221680209499886

Greimann, B. P., & Holly, F. M. (2001). Two-phase flow analysis of concentration profiles. *Journal of Hydraulic Engineering*, *127*(9), 753–762. https://doi.org/10.1061/(ASCE)0733-9429(2001)127:9(753)

Greimann, B. P., Muste, M., & Holly, F. M. (1999). Two-phase formulation of suspended sediment transport. *Journal of Hydraulic Research*, *37*(4), 479–500. https://doi.org/10.1080/00221686.1999.9628264

Hill, K. M., Gaffney, J., Baumgardner, S., Wilcock, P., & Paola, C. (2017). Experimental study of the effect of grain sizes in a bimodal mixture on bed slope, bed texture, and the transition to washload. *Water Resources Research*, *53*, 923–941. https://doi.org/10.1002/2016WR019172

Hsu, T.-J., Jenkins, J. T., & Liu, P. L.-F. (2004). On two-phase sediment transport: Sheet flow of massive particles. *Proceedings of the Royal Society A: Mathematical, Physical and Engineering Sciences*, *460*(2048), 2223–2250. https://doi.org/10.1098/rspa.2003.1273

Jobson, H. (1970). Vertical transfer in open channel flow. *Journal of the Hydraulics Division*, *96*(3), 703–724.

Lamb, M. P., de Leeuw, J., Fischer, W., Moodie, A. J., Venditti, J. G., Nittrouer, J. A., et al. (2020). Mud in rivers transported as flocculated and suspended bed-material. *Nature Geoscience*, *13*, 566–570. https://doi.org/10.1038/s41561-020-0602-5

Lamb, M. P., Dietrich, W. E., & Sklar, L. S. (2008). A model for fluvial bedrock incision by impacting suspended and bed load sediment. *Journal of Geophysical Research*, *113*, F03025. https://doi.org/10.1029/2007JF000915

Lamb, M. P., Nittrouer, J. A., Mohrig, D., & Shaw, J. (2012). Backwater and river plume controls on scour upstream of river mouths: Implications for fluvio-deltaic morphodynamics. *Journal of Geophysical Research*, *117*, F01002. https://doi.org/10.1029/2011JF002079

Lamb, M. P., & Parsons, J. D. (2005). High-density suspensions formed under waves. *Journal of Sedimentary Research*, *75*(3), 386–397. https://doi.org/10.2110/jsr.2005.030

Landau, L. D., & Lifshits, E. M. (1959). *Fluid mechanics*. London: Pergamon Press; Addison-Wesley Pub. Co.

Lees, B. J. (1981). Relationship between eddy viscosity of seawater and eddy diffusivity of suspended particles. *Geo-Marine Letters*, *1*(3–4), 249–254. https://doi.org/10.1007/BF02462442

Leopold, L. B., Wolman, M. G., & Miller, J. P. (1995). *Fluvial processes in geomorphology*. New York: Dover Publications. Dover ed.

Li, C., Czapiga, M. J., Eke, E. C., Viparelli, E., & Parker, G. (2015). Variable Shields number model for river bankfull geometry: Bankfull shear velocity is viscosity-dependent but grain size-independent. *Journal of Hydraulic Research*, *53*(1), 36–48. https://doi.org/10.1080/00221686.2014.939113

Lyn, D. A. (1986). Turbulence and turbulent transport in sediment-laden open-channel flows (PhD Thesis), California Institute of Technology, Pasadena, California.

Ma, H., Nittrouer, J. A., Fu, X., Parker, G., Zhang, Y., Wang, Y., et al. (2022). Amplification of downstream flood stage due to damming of fine-grained rivers. *Nature Communications,* 13. https://doi.org/10.1038/s41467-022-30730-9

Ma, H., Nittrouer, J. A., Naito, K., Fu, X., Zhang, Y., Moodie, A. J., et al. (2017). The exceptional sediment load of fine-grain dispersal systems: Example of the Yellow River, China. *Science Advances*, *12*(3), e1603114. https://doi.org/10.1126/sciadv.1603114

Ma, H., Nittrouer, J. A., Wu, B., Lamb, M. P., Zhang, Y., Mohrig, D., et al. (2020). Universal relation with regime transition for sediment transport in fine-grained rivers. *Proceedings of the National Academy of Sciences*, *117*, 171–176. https://doi.org/10.1073/pnas.1911225116

McElroy, B., & Mohrig, D. (2009). Nature of deformation of sandy bed forms. *Journal of Geophysical Research*, *114*, F00A04. https://doi.org/10.1029/2008JF001220

McLean, S. R. (1991). Depth-integrated suspended-load calculations. *Journal of Hydraulic Engineering*, *117*(11), 1440–1458. https://doi.org/10.1061/(ASCE)0733-9429(1991)117:11(1440)

McLean, S. R. (1992). On the calculation of suspended load for noncohesive sediments. *Journal of Geophysical Research*, *97*(C4), 5759. https://doi.org/10.1029/91JC02933

McLean, S. R., Nelson, J. M., & Wolfe, S. R. (1994). Turbulence structure over two-dimensional bed forms: Implications for sediment transport. *Journal of Geophysical Research*, *99*(C6), 12,729–12,747. https://doi.org/10.1029/94JC00571

Mellor, G. L., & Yamada, T. (1982). Development of a turbulence closure model for geophysical fluid problems. *Reviews of Geophysics*, *20*(4), 851–875. https://doi.org/10.1029/RG020i004p00851

Meselhe, E. A., Georgiou, I., Allison, M. A., & McCorquodale, J. A. (2012). Numerical modeling of hydrodynamics and sediment transport in lower Mississippi at a proposed delta building diversion. *Journal of Hydrology*, *472–473*, 340–354. https://doi.org/10.1016/j.jhydrol.2012.09.043

Milliman, J. D., & Meade, R. H. (1983). World-wide delivery of river sediment to the oceans. *The Journal of Geology*, *91*(1), 1–21. https://doi.org/10.2307/30060512

Minier, J.-P., Chibbaro, S., & Pope, S. B. (2014). Guidelines for the formulation of lagrangian stochastic models for particle simulations of single-phase and dispersed two-phase turbulent flows. *Physics of Fluids*, *26*, 113,303.

Mofjeld, H. O. (1988). Formulas for velocity, sediment concentration and suspended sediment flux for steady uni-directional pressure-driven flow.

Moodie, A. J. (2019). Yellow River Kenli Lijin Station survey [dataset]. https://doi.org/10.5281/zenodo.3457639

Moodie, A. J., Nittrouer, J. A., Ma, H., Carlson, B. N., Chadwick, A. J., Lamb, M. P., & Parker, G. (2019). Modeling deltaic lobe-building and channel avulsions for the Yellow River delta, China. *Journal of Geophysical Research: Earth Surface*, *124*, 2438–2462. https://doi.org/10.1029/2019JF005220

Munk, W. H., & Anderson, E. R. (1948). Notes on a theory of the thermocline. *Journal of Marine Research*, *7*(3), 276–295.

Murray, S. P. (1970). Settling velocities and vertical diffusion of particles in turbulent water. *Journal of Geophysical Research*, *75*(9), 1647–1654. https://doi.org/10.1029/JC075i009p01647

Nezu, I., & Azuma, R. (2004). Turbulence characteristics and interaction between particles and fluid in particle-laden open channel flows. *Journal of Hydraulic Engineering*, *130*(10), 988–1001. https://doi.org/10.1061/(ASCE)0733-9429(2004)130:10(988)

Nezu, I., & Rodi, W. (1986). Open-channel flow measurements with a laser Doppler anemometer. *Journal of Hydraulic Engineering*, *112*(5), 335–355. https://doi.org/10.1061/(ASCE)0733-9429(1986)112:5(335)

Nikuradse, J. (1926). Laws of flow in rough pipes, translation of stromungsgesetze in rauhen rohren (Tech. Rep. No. NACA-TM-1292). Report Date: Nov 01, 1950.

Nittrouer, J. A., Allison, M. A., & Campanella, R. (2008). Bedform transport rates for the lowermost Mississippi River. *Journal of Geophysical Research*, *113*, F03004. https://doi.org/10.1029/2007JF000795

Nittrouer, J. A., Best, J. L., Brantley, C., Cash, R. W., Czapiga, M., Kumar, P., & Parker, G. (2012). Mitigating land loss in coastal Louisiana by controlled diversion of Mississippi River sand. *Nature Geoscience*, *5*(8), 534–537. https://doi.org/10.1038/ngeo1525

Nittrouer, J. A., Mohrig, D., & Allison, M. (2011). Punctuated sand transport in the lowermost Mississippi River. *Journal of Geophysical Research*, *116*, F04025. https://doi.org/10.1029/2011JF002026

Nittrouer, J. A., & Viparelli, E. (2014). Sand as a stable and sustainable resource for nourishing the Mississippi River delta. *Nature Geoscience*, *7*(5), 350–354. https://doi.org/10.1038/ngeo2142

Paola, C., Parker, G., Mohrig, D. C., & Whipple, K. X. (1999). The influence of transport fluctuations on spatially averaged topography on a sandy, braided fluvial fan, *Numerical experiments in stratigraphy: Recent advances in stratigraphic and sedimentologic computer simulations* (pp. 211–218). Society for Sedimentary Geology.

Parker, G., & Coleman, N. L. (1986). Simple model of sediment-laden flows. *Journal of Hydraulic Engineering*, *112*(5), 356–375. https://doi.org/10.1061/(ASCE)0733-9429(1986)112:5(356)
Partheniades, E. (1977). Unified view of wash load and bed material load. *Journal of the Hydraulics Division*, *103*(9), 1037–1057.
Ren, M.-e., & Walker, H. J. (1998). Environmental consequences of human activity on the Yellow River and its delta, China. *Physical Geography*, *19*(5), 421–432.
Rose, C. P., & Thorne, P. D. (2001). Measurements of suspended sediment transport parameters in a tidal estuary. *Continental Shelf Research*, *21*(15), 1551–1575. https://doi.org/10.1016/S0278-4343(00)00087-X
Rouse, H. (1937). Modern conceptions of the mechanics or fluid turbulence. *Transactions of the American Society of Civil Engineers*, *102*(1), 463–505.
Rouse, H. (1939). *An analysis of sediment transportation in the light of fluid turbulence*. Washington, DC: United States Department of Agriculture. https://resolver.caltech.edu/CaltechAUTHORS:20140529-132455484
Saito, Y., Wei, H., Zhou, Y., Nishimura, A., Sato, Y., & Yokota, S. (2000). Delta progradation and chenier formation in the Huanghe (Yellow River) delta, China. *Journal of Asian Earth Sciences*, *18*(4), 489–497. https://doi.org/10.1016/S1367-9120(99)00080-2
Saito, Y., Yang, Z., & Hori, K. (2001). The Huanghe (Yellow River) and Changjiang (Yangtze River) deltas: A review on their characteristics, evolution and sediment discharge during the Holocene. *Geomorphology*, *41*(2–3), 219–231. https://doi.org/10.1016/S0169-555X(01)00118-0
Schmeeckle, M. W. (2014). Numerical simulation of turbulence and sediment transport of medium sand. *Journal of Geophysical Research: Earth Surface*, *119*, 1240–1262. https://doi.org/10.1002/2013JF002911
Smith, J. D., & McLean, S. R. (1977). Spatially averaged flow over a wavy surface. *Journal of Geophysical Research*, *82*(12), 1735–1746. https://doi.org/10.1029/JC082i012p01735
Toorman, E. (2002). Modelling of turbulent flow with suspended cohesive sediment. *Proceedings in Marine Science*, *5*, 155–169. https://doi.org/10.1016/S1568-2692(02)80014-6
Turner, J. S. (1979). *Buoyancy effects in fluids* (1st). Cambridge: Cambridge University Press.
van Gelder, A., van den Berg, J. H., Cheng, G., & Xue, C. (1994). Overbank and channelfill deposits of the modern Yellow River delta. *Sedimentary Geology*, *90*(3–4), 293–305. https://doi.org/10.1016/0037-0738(94)90044-2
van Ingen, C. (1981). Observations in a sediment-laden flow by use of laser-doppler velocimetry, *Tech. Rep. No. KH-R-42*. https://doi.org/10.7907/Z9QF8QTP
van Rijn, L. C. (1984). Sediment transport, Part II: Suspended load transport. *Journal of Hydraulic Engineering*, *110*(11), 1613–1641. https://doi.org/10.1061/(ASCE)0733-9429(1984)110:11(1613)
Vanoni, V. A. (1941). Some experiment on the transporation of suspended load. *Transactions, American Geophysical Union*, *22*(3), 608. https://doi.org/10.1029/TR022i003p00608
Vanoni, V. A. (1946). Transportation of sediment by water. *Transactions of the AGU*, *3*, 67–133.
Villaret, C., & Trowbridge, J. H. (1991). Effects of stratification by suspended sediments on turbulent shear flows. *Journal of Geophysical Research*, *96*(C6), 10,659–10,680. https://doi.org/10.1029/91JC01025
Viparelli, E., Nittrouer, J. A., & Parker, G. (2015). Modeling flow and sediment transport dynamics in the lowermost Mississippi River, Louisiana, USA, with an upstream alluvial-bedrock transition and a downstream bedrock-alluvial transition: Implications for land building using engineered diversions: Alluvial-bedrock-alluvial rivers. *Journal of Geophysical Research: Earth Surface*, *120*, 534–563. https://doi.org/10.1002/2014JF003257
Wang, Z., & Larsen, P. (1994). Turbulent structure of water and clay suspensions with bed load. *Journal of Hydraulic Engineering*, *120*(5), 577–600. https://doi.org/10.1061/(ASCE)0733-9429(1994)120:5(577)
Wang, Z.-Y., & Liang, Z.-Y. (2000). Dynamic characteristics of the Yellow River mouth. *Earth Surface Processes and Landforms*, *25*(7), 765–782. https://doi.org/10.1002/1096-9837(200007)25:7<765::AID-ESP98>3.0.CO;2-K
Whitehouse, R. (1995). Observations of the boundary layer characteristics and the suspension of sand at a tidal site. *Continental Shelf Research*, *15*(13), 1549–1567. https://doi.org/10.1016/0278-4343(95)00038-3
Winterwerp, J. C. (2006). Stratification effects by fine suspended sediment at low, medium, and very high concentrations. *Journal of Geophysical Research*, *111*, C05012. https://doi.org/10.1029/2005JC003019
Woo, H. S., Julien, P. Y., & Richardson, E. V. (1986). Washload and fine sediment load. *Journal of Hydraulic Engineering*, *112*(6), 541–545.
Wright, S., & Parker, G. (2004a). Density stratification effects in sand-bed rivers. *Journal of Hydraulic Engineering*, *130*(8), 783–795. https://doi.org/10.1061/(ASCE)0733-9429(2004)130:8(783)
Wright, S., & Parker, G. (2004b). Flow resistance and suspended load in sand-bed rivers: Simplified stratification model. *Journal of Hydraulic Engineering*, *130*(8), 796–805. https://doi.org/10.1061/(ASCE)0733-9429(2004)130:8(796)
Wright, S., & Parker, G. (2005). Modeling downstream fining in sand-bed rivers. I: Formulation. *Journal of Hydraulic Research*, *43*(6), 613–620. https://doi.org/10.1080/00221680509500381
Xu, K., Bentley, S. J., Day, J. W., & Freeman, A. M. (2019). A review of sediment diversion in the Mississippi River Deltaic Plain. *Estuarine, Coastal and Shelf Science*, *225*, 106241. https://doi.org/10.1016/j.ecss.2019.05.023
Yeh, T.-h., & Parker, G. (2013). Software for evaluating sediment-induced stratification in open-channel flows. *Computers & Geosciences*, *53*, 94–104. https://doi.org/10.1016/j.cageo.2011.12.004
Yu, L. (2002). The Huanghe (Yellow) River: A review of its development, characteristics, and future management issues. *Continental Shelf Research*, *22*(3), 389–403. https://doi.org/10.1016/S0278-4343(01)00088-7
Zhang, S., & Duan, J. G. (2011). 1D finite volume model of unsteady flow over mobile bed. *Journal of Hydrology*, *405*(1–2), 57–68. https://doi.org/10.1016/j.jhydrol.2011.05.010
Zhang, S., Duan, J. G., & Strelkoff, T. S. (2013). Grain-scale nonequilibrium sediment-transport model for unsteady flow. *Journal of Hydraulic Engineering*, *139*(1), 22–36. https://doi.org/10.1061/(ASCE)HY.1943-7900.0000645